

# **An Actively Stabilised Model Rocket**

by  
*David Wyatt (TH)*

*Fourth-year undergraduate project in  
Group C, 2006/2007*

"Hofstadter's Law: It always takes longer than you expect, even when you take into account Hofstadter's Law."

- Douglas Hofstadter, *Gödel, Escher, Bach: An Eternal Golden Braid*

I hereby declare that, except where specifically indicated, the work submitted herein is my own original work.

# Table of Contents

1 Introduction.....	1
2 Top-level design.....	3
2.1 Concept selection.....	3
2.2 Control system architecture.....	5
2.3 Safety.....	6
3 Mechanical design.....	7
3.1 Motor selection and flight simulation.....	7
3.2 Thruster force.....	8
3.3 Airframe design.....	8
4 Pneumatics system.....	11
4.1 Overall pneumatics system design.....	11
4.2 Gas supply.....	11
4.3 Thruster nozzle design.....	12
4.4 Valve selection.....	14
4.5 PWM frequency selection.....	15
5 Electronic design.....	16
5.1 Processor selection.....	16
5.2 Attitude sensor selection.....	17
5.3 Power supply.....	18
5.4 Circuit design.....	18
6 Software and control.....	19
6.1 System model.....	19
6.2 Rate gyro sensor inputs.....	20
6.3 Control law.....	20
6.4 Simulation.....	22
6.5 Software structure.....	24
6.6 Development environment and toolchain.....	25
7 Construction and testing.....	25
7.1 Time and expenditure.....	25
7.2 Phase 1: Turntable testbed.....	26
7.3 Phase 2 & 3 airframe construction.....	28
7.4 Mass reduction.....	29
7.5 Bench tests.....	30
7.6 Maiden flight.....	32
8 Conclusions.....	35
8.1 Project achievements and validity of concept.....	35
8.2 Project significance.....	36
8.3 Evaluation of approach.....	36
8.4 Future work.....	37
9 Acknowledgements.....	39
10 References.....	40
Appendix A: Structural design of primary truss and landing legs.....	43
Appendix B: Thruster nozzle final design.....	45
Appendix C: Requirements for rocketry avionics.....	46
Appendix D: Avionics circuit diagrams and circuit board layouts.....	47
Main avionics board.....	47
Valve driver board.....	48
Gyro board.....	48
Photographs of assembled circuit boards.....	49

# 1 Introduction

Rockets – like many aerospace systems, or indeed any structure travelling in free fall – are inherently unstable in flight, in that any external disturbance or internal misalignment of the thrust vector with the centre of mass will cause the vehicle to deviate from its intended path, and any restoring force must be provided by the vehicle itself. The principal source of disturbance forces in the absence of aerodynamic loads is misalignment of the thrust vector with the centre of mass, as shown in Figure 1; reaction forces (e.g. from explosive lower-stage separation) may also be important.

To combat this problem, conventional rockets and missiles from the Second World War onwards have used “active stabilisation”: electromechanical control systems to detect such deviations from the predetermined path and correct for them. A wide range of these systems has been developed (see section 2.1).

This contrasts with smaller rockets (scientific sounding rockets and hobbyists' constructions) which use passive stability through aerodynamic effects as shown in Figure 2. The distributed aerodynamic drag may be considered as a point force acting at the “centre of pressure” (CoP); if the CoP is behind the centre of mass (CoM), achieved by placing ballast in the nose of the rocket and fixed fins at the rear, the drag force produces a restoring torque to bring the two into line and aerodynamic forces provide damping. If a disturbance torque is applied (e.g. through thrust vector misalignment) the drag force, and thus the air speed of the vehicle, must be sufficient to overcome it – thus passive stabilisation works only at high speeds. The technique is also only feasible on smaller rockets (due to the fin sizes that would be necessary on larger vehicles), but it is immeasurably simpler to implement than active stabilisation; indeed, the complexity and expense of the latter, coupled with the small size of hobby rockets, means that amateur actively-stabilised rockets have rarely been built in the past ([1], [2]).

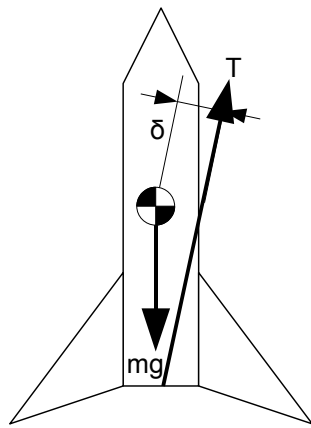


Figure 1: Rocket flight dynamics in the absence of aerodynamic forces. In general it is impossible to ensure perfect alignment of the thrust vector with the centre of mass – thus a disturbance torque of magnitude  $T\delta$  is created, which if uncorrected will lead to accelerating rotation of the vehicle.

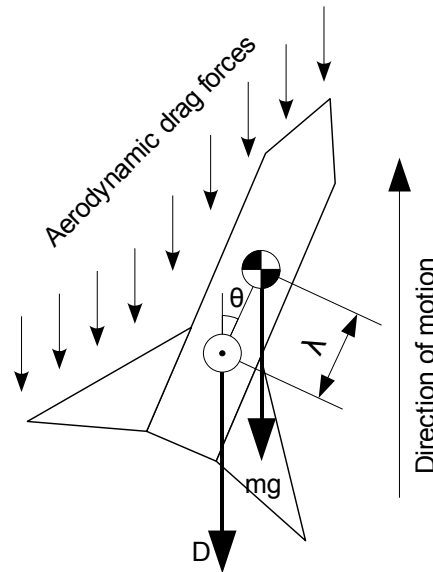


Figure 2: Passive aerodynamic stability. The centre of pressure is denoted  $\odot$ . A torque  $D\lambda\sin\theta$  seeks to drive  $\theta$  to 0. In general, the larger the distance  $\lambda$  the more stable the rocket.

However, passive stabilisation has certain disadvantages:

1. A common aim in hobby rocketry is breaking apogee altitude records. Here passive stability can be a hindrance on a windy day as it causes rockets to turn into the wind (“weathercocking”), reducing their apogee height and increasing the drift distance from the launch point. An active stabilisation system fitted to a high-power hobby rocket would allow vertical flight even in windy conditions and could reduce lateral drift.
2. Non-aerodynamic attitude control systems are obligatory for vehicles that operate outside the atmosphere – for example, landing on the lunar surface. NASA's recent Vision for Space Exploration ([3]) involves the development of hovering rocket-powered lunar landers, to which end the agency made development of a such a vehicle one of its Centennial Challenges with a \$2 million prize ([4]). On a smaller scale, Cambridge University Spaceflight's Martlet project ([5]) aims to launch a small rocket from a weather balloon at an altitude of 30km; since the density of air at this altitude is 1.5% of that at sea level ([6]), and thus the stabilising aerodynamic forces are significantly reduced, non-aerodynamic stabilisation is one of the options under

consideration.

The goal of this project, therefore, is the design and construction of a small (hobby-scale) actively-stabilised rocket that uses non-aerodynamic means to effect stabilisation about the pitch and yaw axes (for the definition of pitch, yaw and roll, see Figure 3); control of the roll axis of the rocket was not required as that axis does not affect its stability in flight. Commercially-available components and materials were used wherever possible, both for reasons of cost and to allow this project's achievements to be replicated elsewhere. Maximising apogee height was not be considered; instead, the aim is to maintain a long stable flight at a low altitude.

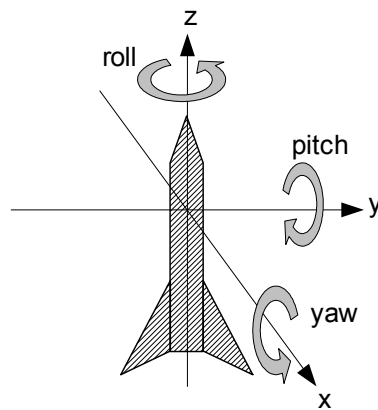


Figure 3: The pitch, yaw and roll axes of a rocket

## 2 Top-level design

### 2.1 Concept selection

Numerous methods of non-aerodynamic attitude stabilisation and control have been implemented over the history of spaceflight; Table 1 describes some of the main methods (partially taken from [7]). Other methods that have been used in large-scale vehicles in the past include: jet tabs, the jetavator, fluidic steering and control moment gyros; however, it was judged that they were not practical for this project.

The concepts are scored in Table 2 for their applicability in this context. The two most promising concepts - "gimballed engine" and "attitude thrusters" - were investigated in more detail leading to CAD mock-ups, renderings of which are shown in Figure 4 and Figure 5 respectively, and refinements of the scores for these

concepts. Using the scores and weightings indicated, attitude thrusters were chosen as the most appropriate concept to pursue; in contrast, previous hobby rockets using non-aerodynamic active stabilisation ([1], [2]) have employed the “gimballed engine” method.

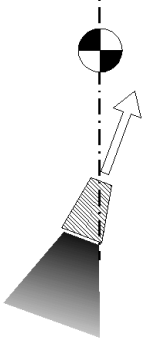
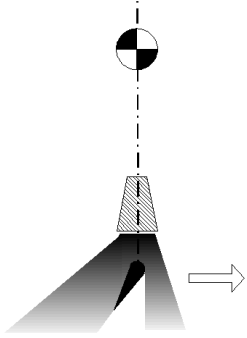
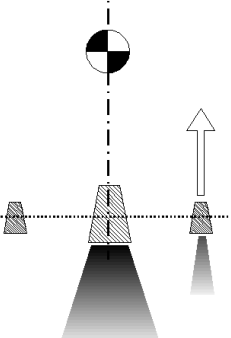
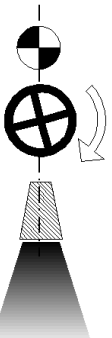
	<u>Gimballed engine</u>	<u>Jet vanes</u>	<u>Attitude thrusters</u>	<u>Reaction wheels</u>
<b>Diagram</b>				
<b>Description</b>	Main engine(s) is/are offset from the centre of mass with actuated rotary degrees of freedom, producing control moments by tilting the thrust vector.	Aerodynamic vanes of a refractory material are placed in the exhaust plume of the rocket to redirect it and (by reaction) exert torques on the vehicle.	Small throttlable thrusters are offset from the centre of mass and activated selectively to provide control moments.	Heavy flywheels are accelerated or decelerated to provide (by reaction) control moments about their axes.
<b>Examples</b>	Black Arrow, Saturn IB/V, Space Shuttle (main engines), Apollo Lunar Module (descent stage), hobby rockets: Gyroc ([1]), Casimiro ([2])	Early Goddard rockets, V2 missile	Satellites, Apollo Lunar Module (ascent stage), Space Shuttle (reaction control system), Harrier aircraft	Satellites, Murata Boy balancing robot ([8])

Table 1: Concepts for non-aerodynamic attitude control

Criterion	Weight	Concept			
		Gimballed main engine	Jet vanes	Attitude thrusters	Reaction wheels
Cost	2	DATUM	0	0	-1
Applicability to hobby rockets	2		1	-1	-2
Simplicity of design	3		-2	1	-1
Simplicity of construction	3		-1	1	0
Robustness & reliability	3		-1	1	0
Mass	2		0	-1	-2
Independence from rocket motor	3		0	1	1
<b>Total score</b>			<b>0</b>	<b>-10</b>	<b>8</b>

Table 2: Attitude control system concept evaluation

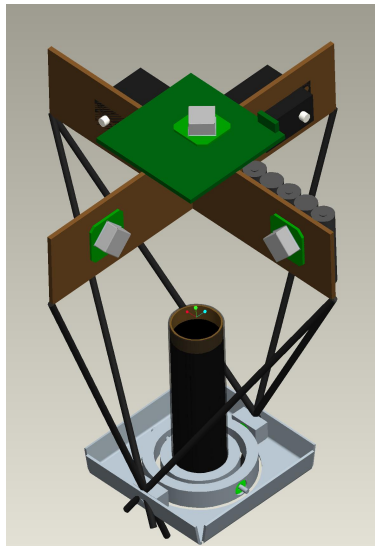


Figure 4: Mockup of a rocket with a gimbaled engine. The motor is the black cylinder in the centre of the gimbals in the lower part of the vehicle; a lightweight truss separates it from the upper section, which houses the avionics (3 gyros and a circuit board are indicated), two hobby servomotors to actuate the gimbals and a battery pack.

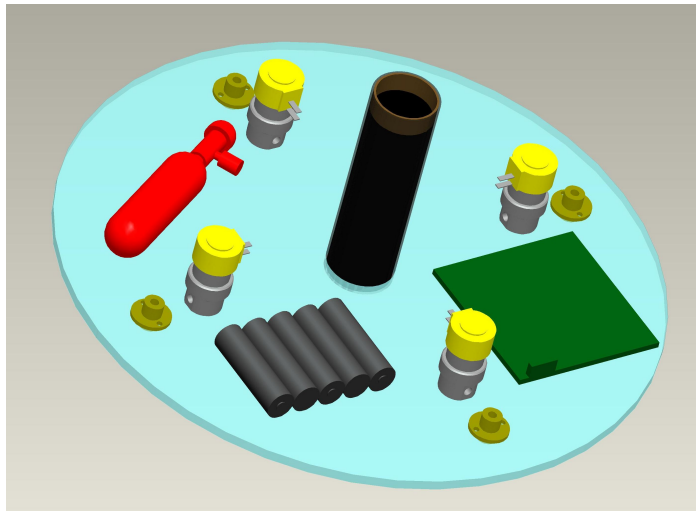


Figure 5: Mockup of a rocket with attitude thrusters. The motor is the black cylinder in the centre of the baseplate; it is surrounded by four solenoid valves and four thruster nozzles (towards the edge of the plate). Other components shown include the gas cylinder and regulator, a battery pack and the avionics circuit board.

## 2.2 Control system architecture

The functional architecture of the attitude-thruster-based control system is shown in Figure 6. The microcontroller reads the angular velocity values from the pitch and yaw rate gyros over the SPI serial bus ([9]) to estimate the current state (orientation and angular velocities) of the vehicle. The control law is then applied to the estimated state to derive thruster commands in the form of torques about the

pitch and yaw axes. The flow of compressed gas to the thruster nozzles is governed by solenoid valves, driven by the thruster commands from the microcontroller. A log is kept of all key variables in non-volatile memory on a Secure Digital card to allow debugging and future development of the control system; this communication also takes place over the SPI bus.

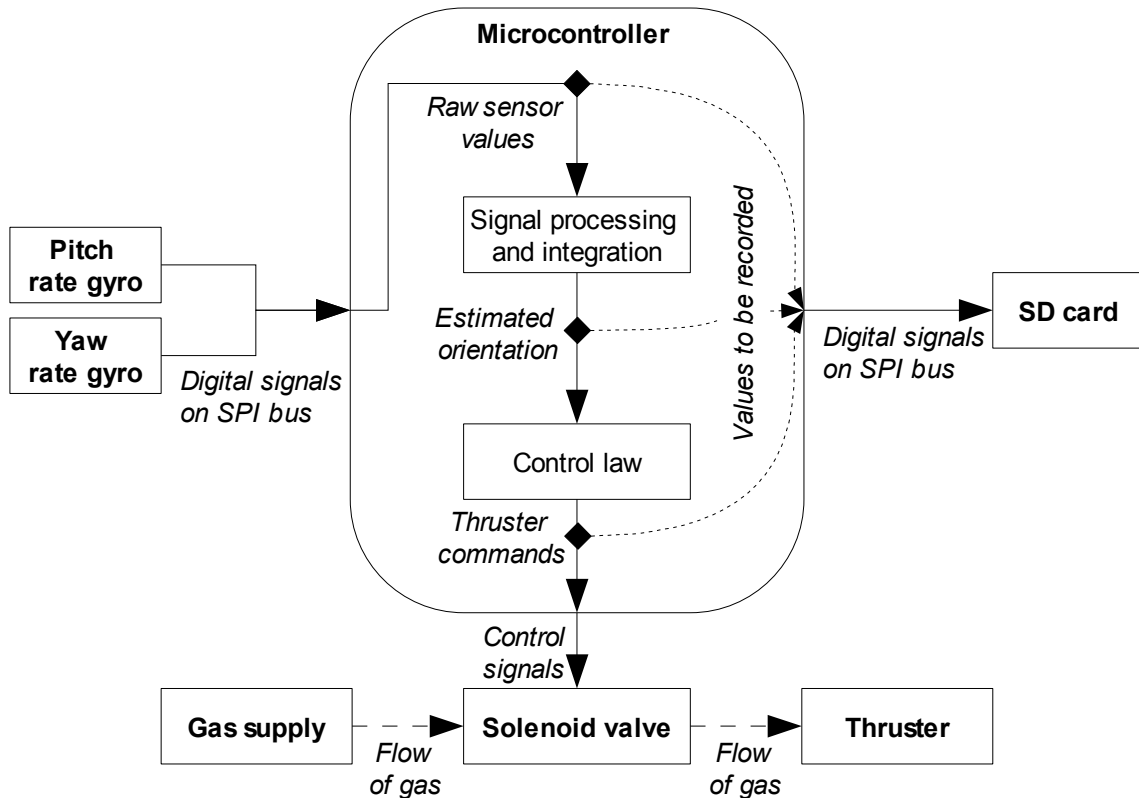


Figure 6: Control system architecture. In the complete system there are multiple solenoid valves and thrusters; for clarity, only one of each is shown.

### 2.3 Safety

Safety considerations have been paramount throughout the project. As well as submitting a comprehensive risk assessment to Cambridge University Engineering Department, the UK Rocketry Association (UKRA)'s published Safety Code ([10]), in particular the section relating to experimental rockets, has been adopted and permission was sought from the UKRA Safety and Technical Committee before flying. The first test flight was held at an East Anglia Rocketry Society (EARS, [11]) launch day under the supervision of a designated Range Safety Officer, and all spectators were made aware of the potential risks before launch. Calculations were

also undertaken to establish the ballistic range achievable, for the purposes of establishing a safe distance for spectators. Since the flight profile (see section 3.1) involves an initial impulsive acceleration to 1.4m/s followed by a prolonged coast under a net acceleration of approximately 0.1g, standard formulae for ballistic motion of projectiles can be used to estimate the maximum range (achieved for a launch angle of 45°):

$$\begin{aligned}v_{y, initial} + 0.5 a_y t_{landing} &= 0 \\r_{max} &= v_{x, initial} t_{landing} \\v_{x, initial} &= v_{y, initial} = v_{initial} / \sqrt{2}\end{aligned}$$

With  $v_{initial} = 1.4\text{m/s}$  and  $a_y = -0.981\text{m/s}^2$ , this gives  $t_{landing} = 2.03\text{s}$  and  $r_{max} = 2.03\text{m}$

In the event of a side wind, the rocket may drift and travel further than this distance. Using conservative assumptions of a drag coefficient ( $C_D$ ) of 1, a cross-sectional area of  $0.03\text{m}^2$  and a wind speed of  $5\text{ms}^{-1}$ , it was estimated that the rocket might travel 1.8m during the course of a 3s flight.

## 3 Mechanical design

### 3.1 Motor selection and flight simulation

The rocket motor taken as the baseline for this project is the Estes E9-P, with a total impulse of 28.5Ns, a burn time of 3.09s and an average thrust of 9N ([12]). Since the thrust curve of the rocket motor is fixed (to within manufacturing tolerances, a standard deviation of around 6% for this motor according to [13]), and since aerodynamic forces are relatively unimportant at the low flight speeds at which the vehicle will operate, the main variable affecting the flight profile is the rocket's mass. Flight profiles were simulated in Matlab for a range of masses (disregarding drag) using a sample E9-P thrust curve from [13]; the results are shown in Figure 7. For a lift-off mass of over 1.030kg the flight ends before motor burnout, which is potentially dangerous. However, it is desirable to minimise the landing velocity to avoid damage to the vehicle's components. A nominal mass of 1.01kg was thus chosen, giving an apogee height of 1.5m and landing velocity of 4.3m/s. The flight

profile for this mass is shown in Figure 8.

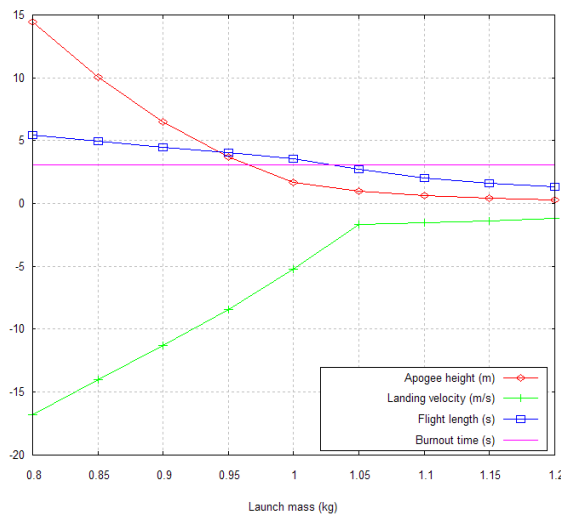


Figure 7: Modelled variation of flight parameters with mass. The sharp “kink” in the landing velocity curve corresponds to the mass at which the rocket lands before motor burnout (the solid purple line indicates the turnout time in seconds).

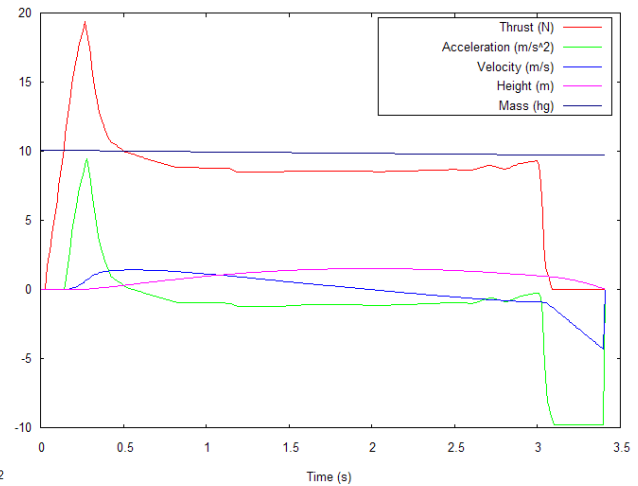


Figure 8: Modelled flight profile for a 1.01kg rocket. Since the thrust is approximately constant during the plateau and slightly less than the rocket's weight, after the initial thrust peak the vehicle's motion resembles a parabola in 12% gravity. At motor burnout the rocket is 0.9m off the ground and free-falls to impact.

It was recognised that a longer flight could be achieved by using longer-burning motors with approximately the same thrust level as the Estes E9-P. One option is the Aerotech G12-RCT [14], with a thrust of about 9N maintained over 8 seconds. An alternative non-explosive form of propulsion would be an electric ducted fan mounted in place of the rocket engine.

### 3.2 Thruster force

To set specifications for the thruster torque, the radius of gyration was estimated to be 5cm. In order to translate horizontally by 5m in 2s (during the steady-thrust section of the E9-P's burn time), the vehicle would have to tilt by 34°; allowing a tilt manoeuvre time of 0.2s implies that the maximum thruster torque should be 0.15Nm, corresponding to a 0.75N thruster on a 0.2m moment arm. Thus the nominal thruster force for design purposes was chosen to be 1N to leave a margin for manufacturing imperfections.

### 3.3 Airframe design

Since a streamlined shape for the rocket was not required, there was great freedom in the mechanical design of the airframe. The overall design objective was to

keep the moment of inertia small for a thruster moment arm of 0.2m, while accommodating all the components of the rocket and achieving sufficient robustness to survive the shock of landing.

Two alternative layouts for the pitch and yaw thrusters relative to the centre of mass were considered. These are depicted and described in Table 3. To simplify the control system, the “Maltese” design was chosen as manufacturing tolerances were less likely to lead to cross-coupling between the pitch and yaw axes and the vertical force exerted by the thrusters could be used to decelerate the rocket on landing.

Design	“Missile”	“Maltese”
<b>Diagram</b> (side view (showing centre of mass) and base view; rocket motor nozzle shown in black, thruster nozzles shown in dark grey)		
<b>Proposed structural materials</b>	Fibreglass tube	Sheet aluminium/ polymer, kite spar truss
<b>Linear motion direction affected by thrusters</b>	Horizontal	Vertical
<b>Axis most affected by pitch thruster misalignment*</b>	Yaw	Roll
<b>Effect of side wind</b>	High	Low
<b>Roll moment of inertia</b>	Low	High
<b>Robustness on impact</b>	High	Low

Table 3: Comparison of alternative mechanical layouts for the vehicle. \*Misalignment of a pitch thruster will cause its thrust to have components with moments about the yaw and roll axes; assuming misalignment errors are equal in these two directions, the axis about which the thruster has the greatest moment arm will be most affected; in the “Missile” design this is the yaw axis while in the “Maltese” design this is the roll axis. Similarly, yaw thruster misalignment principally affects the pitch axis in the “Missile” design and the roll axis in the “Maltese” design.

The above considerations led to a design consisting of a central box made from sheet aluminium, compactly housing the dense components of the rocket (the rocket

motor, solenoid valves, batteries, gas supply and avionics); and four identical fibreglass/carbon-fibre kite spar truss structures supporting the thrusters and landing legs at their tips. The rocket motor mount was designed to accept either the 32mm diameter Aerotech G12-RCT motor ([14]) or, via an adapter, the 24mm diameter Estes E9-P motor ([12]).

To accommodate a worst-case landing condition, the trusses were designed using static equilibrium, pin-jointed truss analysis and Euler buckling so that each could support an upwards load of 100N at the tip (corresponding to a single landing leg decelerating a 1kg mass from 5m/s to rest in 0.1s with a peak force twice the average). Full details of the calculations are provided in Appendix A. As well as the inelastic collision between the landing leg and the ground, additional energy absorption would be effected if necessary by elastic buckling of the truss segments and shear failure of the (replaceable) nylon screws.

A CAD rendering of the mechanical design is shown in Figure 9.

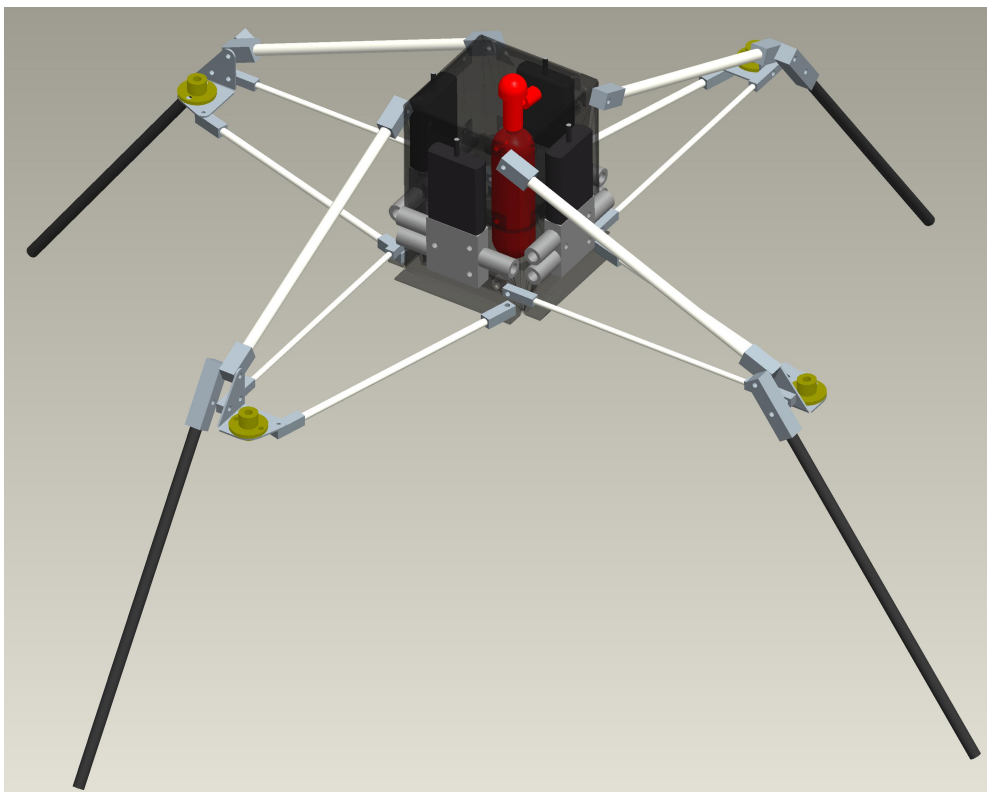


Figure 9: A CAD rendering of the mechanical design of the rocket. The central box (translucent dark grey) is made from sheet aluminium and houses the rocket motor, batteries and gas cylinder (red); the four solenoid valves (black and grey) are mounted on its exterior faces. The thrusters (yellow) are supported at the ends of the primary fibreglass kite spar truss (white), to which the CFRP kite spar landing legs are also attached. Pneumatic tubing and avionics are not shown – the latter are secured to the top surface of the central box.

## 4 Pneumatics system

### 4.1 Overall pneumatics system design

The function of the pneumatics system is to distribute a throttleable flow of high-pressure gas from a supply to a number of attitude thrusters. In this case four attitude thrusters were used, a pair each for pitch and yaw.

Throttle control is given by on-off solenoid valves, driven with a pulse-width-modulation (PWM) waveform from the microcontroller; this allows the effective thrust to be varied continuously from zero to the thrust from a constantly open valve by changing the duty cycle. The alternative would have been the use of “proportional” solenoid valves which give a flow rate that varies with the solenoid current; however, since the dynamics of the rocket approximate a low-pass filter the PWM method can be used, and PWM has the advantages of more efficient use of gas (the input flow to the thruster nozzle is at a constant high pressure while the valve is open, giving a higher average specific impulse) and lower component cost.

### 4.2 Gas supply

The gas supply for the attitude thruster system consists of a small cylinder containing 16g of liquid carbon dioxide, commercially available for the inflation of bicycle tyres [15]. Such cylinders are designed to be disposable, using a special fitting to pierce the seal on the cylinder as it is screwed in.



Figure 10: A 16g disposable cylinder of liquid carbon dioxide, of the type used for this project, and a fitting to attach it to a bicycle tyre. The fitting pierces a seal on the stem of the cartridge when screwed on.

The vapour pressure of CO<sub>2</sub> at 284K is 45.3atm [16]; in order to use readily-available pneumatics fittings and valves (which are designed to run at pressures of

up to 10bar for industrial pneumatics applications) a miniature pressure regulator is used as the first component in the circuit, immediately after the gas bottle and fitting. This also eliminates the reduction in pressure as the cylinder empties, which would cause the effective gain of the control system to reduce over time.

### 4.3 Thruster nozzle design

The analysis in this section follows the method from [7], which assumes steady uniform isentropic one-dimensional flow of an ideal gas. This was justifiable in this project since the nozzles are small (meaning that startup transients are short), pressures and temperatures are near ambient and the accelerating nozzle flow would reduce the thickness of the boundary layer such that it would not have an effect.

The thrust from a nozzle consists of two terms, the impulse thrust (the reaction to the expulsion of exhaust gases, equal to the mass flow rate multiplied by the exhaust velocity) and the pressure thrust, as shown in the following equation (terms at the exit of the nozzle are denoted by the subscript “e”):

$$F = \dot{m} v_e + A_e (p_e - p_{atm})$$

It may be shown that the maximum thrust for a given supply pressure is achieved when the exhaust gas supply is expanded to ambient pressure, meaning that the pressure thrust is zero. This may be achieved using a converging-diverging de Laval nozzle: the inlet flow is compressed while at subsonic velocities in the converging section of the nozzle, reaches sonic velocity at the throat and expands supersonically in the diverging section.

The efficiency of a rocket motor can be measured by its specific impulse - the impulse delivered by a given mass of propellant divided by its weight:

$$I_{sp} = \frac{m v_e}{m g} = \frac{v_e}{g}$$

The theoretical specific impulse of CO<sub>2</sub> at 5bar above atmospheric pressure exhausting to atmospheric pressure is 41s (for comparison, the specific impulse of solid fuel rocket motors ranges from 196s to 304s and liquid propellants can achieve specific impulses of 432s in the case of hydrogen-oxygen combustion ([17])). Without the pressure reduction (operating in “blowdown” mode, as many satellite attitude

control systems function) the specific impulse would be 53s – however, such operation would be impractical in this application for the reasons outlined above.

For this design it was assumed that the inlet gas pressure was 5bar above atmospheric at a temperature of 293K and that a thrust of 1N was required. The exhaust velocity for this ratio of pressures is given by:

$$v_e = \sqrt{\frac{2\gamma}{\gamma-1} R T_{supply} \left( 1 - \left( \frac{p_{atm}}{p_{supply}} \right)^{\frac{\gamma-1}{\gamma}} \right)} = 401 \text{ ms}^{-1}$$

This then determines the mass flow rate of gas required for a given thrust:

$$\dot{m} = \frac{F}{v_e} = 2.49 \times 10^{-3} \text{ kgs}^{-1}$$

The required throat area (the area over which the sonic velocity is reached) can then be calculated from:

$$A_{throat} = \dot{m} \frac{\sqrt{R T_{supply}}}{\Gamma p_{supply}} = 1.46 \times 10^{-6} \text{ m}^2$$

where  $\Gamma$  is the Vandekerckhove function:

$$\Gamma = \sqrt{\gamma} \left( \frac{2}{\gamma+1} \right)^{\frac{\gamma+1}{2(\gamma-1)}}$$

The exit area of the nozzle can then be calculated from continuity and De Saint Venant's equation:

$$A_e = \frac{\Gamma}{\sqrt{\frac{2\gamma}{\gamma-1} \left( \frac{p_{atm}}{p_{supply}} \right)^{\frac{2}{\gamma}} \left( 1 - \left( \frac{p_{atm}}{p_{supply}} \right)^{\frac{\gamma-1}{\gamma}} \right)}} A_{throat} = 2.23 \times 10^{-6} \text{ m}^2$$

The corresponding throat and exit diameters are 1.4mm and 1.7mm respectively; a 16g cylinder would last 6.4s with a carbon dioxide consumption of 2.5g/s.

Four valves were fabricated to these specifications by Mechanics Lab technicians; an engineering drawing and photograph of the valve are shown in Appendix B. Under tests, the nozzle produced 0.83N using carbon dioxide at 5bar; a supply pressure of 7bar was needed to give the full 1N of thrust.

#### 4.4 Valve selection

The solenoid valves control the flow of carbon dioxide from the gas supply to the thruster nozzles. Selection criteria for the valves included low mass, high input pressure rating and high flow coefficient  $k_v$  (implying a low pressure loss across the valve) as well as low cost; in particular, the valve is required to supply 2.5g/s of carbon dioxide at 5bar (gauge pressure) to the thruster. These values are shown for small solenoid valves from a range of different manufacturers in Table 4 (data obtained from manufacturers' data sheets); Figure 12 shows a scatter plot of the flow coefficient and pressure rating of these valves, together with a portion of the boundary of the selection criterion. As can be seen, a number of valves are eligible for selection based on these two properties; of these, the valve chosen was the MHE2 produced by Festo [18], on the grounds of mass and cost.

<b>Manufacturer and name</b>	<b>Maximum pressure (bar)</b>	<b><math>k_v</math> value</b>	<b>Mass (kg)</b>
Clippard ET	7	0.07	0.07
Dynamco dash-1 D1K, 1.6mm orifice	10	0.57	0.05
Dynamco dash-1 D1M, 2.3mm orifice	5	1.14	0.05
Flo-control N series 1.6mm orifice Al body	7.5	1.1	0.1
Flo-control N series 2.0mm orifice Al body	4.5	1.5	0.1
Flo-control N series 2.4mm orifice Al body	4	2	0.1
Metalwork PIV.I in-line valve 2.4mm orifice	6.5	2	0.14
Festo MHE2	8	1.39	0.06
Festo MHE3	8	2.78	0.12

Table 4: Properties of small solenoid valves from a range of manufacturers

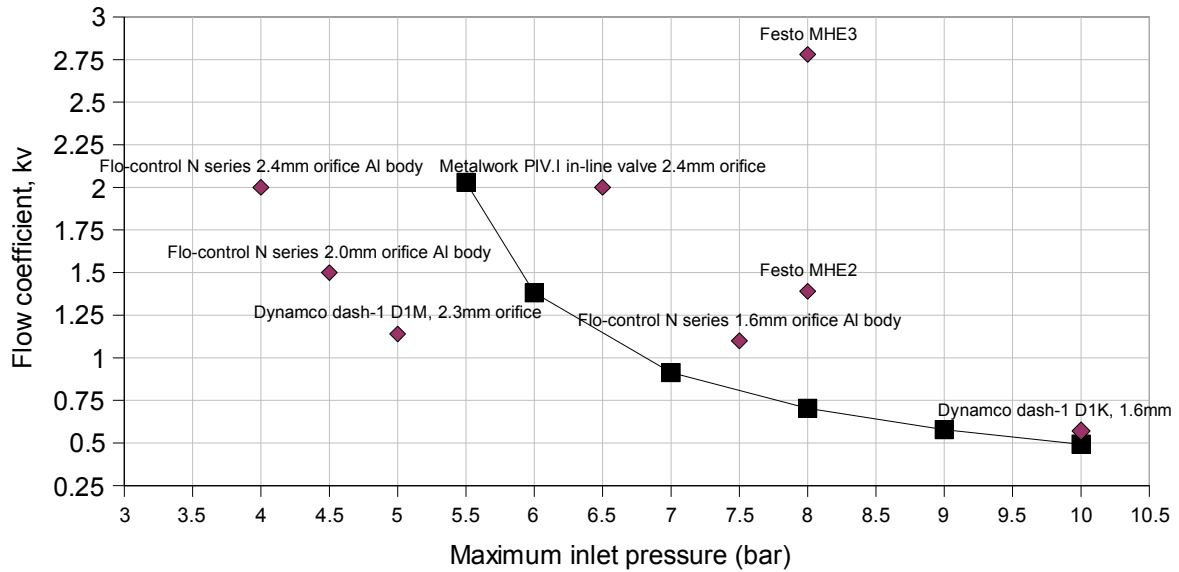


Figure 11: A scatter plot of the flow coefficient and pressure rating of small solenoid valves from a range of different manufacturers. The solid squares, and the lines joining them, represent the boundary of the selection criterion for maximum inlet pressure and flow coefficient; valves above and to the left of the line are acceptable.

#### 4.5 PWM frequency selection

Tests were conducted to determine the relationship between average thrust and PWM waveform properties. The Festo MHE2 valves responded to PWM at frequencies up to 300Hz; a high PWM frequency is desirable as it enables a faster response of the control system and reduces the likelihood of exciting structural vibration in the vehicle. However, with increasing PWM frequencies the relationship between duty cycle and average thrust was found to become increasingly nonlinear, as shown in Figure 12; this is assumed to be due to the inertia of the valve spool, which will act as a low-pass filter to attenuate the harmonic components of the PWM waveform that define the duty cycle. As a compromise between nonlinearity and performance, a PWM frequency of 50Hz was chosen.

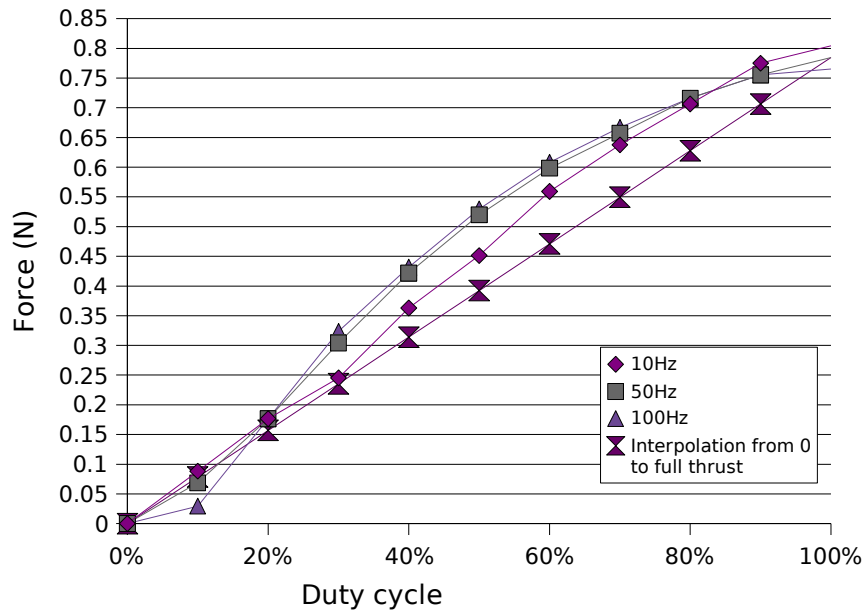


Figure 12: The average force exerted by a thruster nozzle as a function of the duty cycle, for a number of different frequencies. The solenoid valve used was the Festo MHE2; the workshop compressed air supply was used with a nozzle entry pressure of 4bar. A linear interpolation between zero and the maximum thrust achieved is also plotted.

## 5 Electronic design

### 5.1 Processor selection

The onboard processor for the vehicle is a vital part of the digital control system; if during development it was discovered to lack a necessary capability, replacing it with one that did would likely involve significant changes to the hardware and software associated with the project. In order to avoid this, and also to develop expertise that would be useful for future projects requiring similar hardware, the union of the estimated future capabilities required for this project and other proposed rocketry-related projects were taken as a minimum specification when selecting the processor; in particular, the number of analogue input channels and the speed requirement restricted the choice significantly. The full specification is listed in Appendix C.

The processor selected was the LPC2138 ([19]) (an ARM7-TDMI core with a variety of onboard peripherals), produced by NXP Semiconductor ([20]). This device was chosen since it not only met the criteria set but was also readily available from Embedded Artists ([21]) as a module with support circuitry, an RS232 connector and

onboard non-volatile storage, reducing the electronic design and assembly complexity.

## 5.2 Attitude sensor selection

Attitude stabilisation first requires attitude determination about the two stabilised axes of the vehicle (pitch and roll). In general, the rotation of a platform can be measured by a number of means ([17]): either by tracking external phenomena (celestial bodies or the ambient magnetic field direction) or by measuring the inertial effect of rotation. In the latter case, several different technologies exist, all collectively known as “gyroscopes” - a comprehensive overview is given in [22].

The smallest and lightest gyros available are of the “vibrating structure” type; in these, the sensor measurement is derived from the Coriolis acceleration's effect on a micromachined structure that is driven to oscillation (see [23] for a description of the different ways in which such sensors may be constructed).

Several manufacturers produce such devices, including Murata, Silicon Sensing, NEC-Tokin, Gyration and Analog Devices. The selected component was the ADIS16250 produced by Analog Devices ([24], [25]), whose built-in analogue-to-digital conversion (ADC) and calibration features simplified the development of the control system. A picture of the sensing element from this gyro is shown in Figure 13.

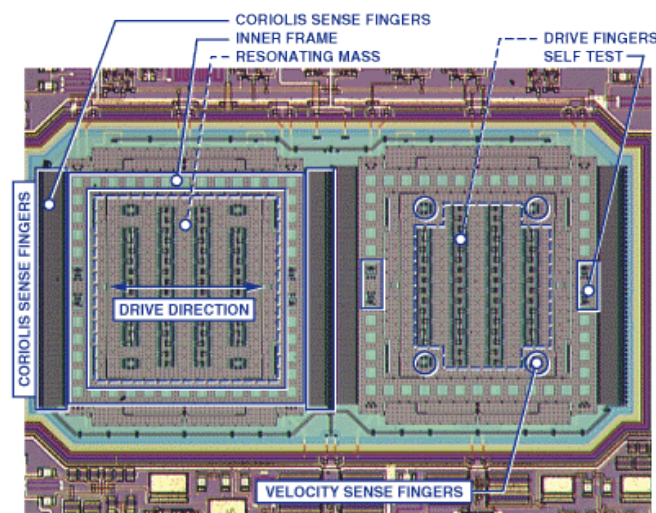


Figure 13 (taken from [26]): A closeup of the sensing element from the Analog Devices ADXRS/ADIS series of micromachined rate gyros. The resonating mass oscillates horizontally within the inner frame; the Coriolis force induced by this causes the inner frame to oscillate vertically, which is detected by the Coriolis sense fingers. The two identical sensing elements oscillate in antiphase, allowing the control electronics to remove common-mode noise (e.g. due to external shock).

### **5.3 Power supply**

The electrical power supply for the vehicle is required to provide 5V at under 400mA for the processor and sensors and 24V at up to 1A for the solenoid valves, while simultaneously being light in weight and small in volume. After examining a number of options, including a step-up converter from low-voltage rechargeable cells and a series interconnection of primary (non-rechargeable) cells, a decision was made to use lithium polymer battery packs specifically designed for electric model aviation, due to their high voltage output and high energy density. The battery packs used were manufactured by Thunder Power ([27]) and are rated to produce 11.1V at up to 9A; two connected in series supply the solenoid valves, while a voltage regulator produces 5V for the logic. The comparatively low capacity of the battery packs (730mAh) is not an issue thanks to the short duration of the flight.

### **5.4 Circuit design**

Initial prototyping of the interface between the processor and the other components was carried out using a development board supplied by the manufacturer of the processor module [21].

Thanks to the integration of the processor and other supporting components on the processor module, the majority of the avionics circuit design constituted interconnection. The avionics functions are divided between three groups of circuit modules:

1. The main avionics board, holding the processor module, voltage regulator, DIP switches for input, LEDs and a piezoelectric buzzer for output, a slot for an SD card for datalogging, as well as connectors for the other boards.
2. The valve driver board, holding four power MOSFETS to interface the processor to the solenoid valves. (The circuit for this board was designed by Gary Bailey.)
3. The two gyro boards, each carrying a single rate gyro and a connector, to be mounted in appropriate orientations to the airframe. (The circuit and layout for these boards were designed by Gary Bailey, who also assembled them.)

Standard 2.54mm pitch Molex crimp connectors were used throughout, to allow

for easy assembly and modification of the wiring harness.

The rate gyros and the SD card are connected to the processor's SPI bus [9] and the four valves were connected to four channels of the processor's built-in PWM generator. The remaining input and output devices on the circuit board are connected to general-purpose input/output (GPIO) pins. Programming and debugging of the microcontroller was carried out through the processor module's built-in RS232 connector; when the avionics board was under test outside of the vehicle, the circuit was also powered from the 5V supply provided by a USB connection.

For safety reasons, the avionics did not control the ignition of the rocket motor to avoid accidental triggering of the launch circuit. Instead, a pair of microswitches are wired in series and attached to two opposite landing legs such that the switches are closed when the legs are in contact with the ground; when either of the microswitches loses contact with the ground, one of the processor's GPIO pins was pulled high to trigger the stabilisation control loop.

Circuit diagrams and printed circuit board layouts for the avionics are shown in Appendix D.

## **6 Software and control**

### **6.1 System model**

It was determined from a CAD model of the mechanical components of the vehicle that the moments of inertia around the pitch and yaw axes were approximately identical; moreover, the off-diagonal terms in the moment of inertia tensor were at least a factor of 200 less than the diagonal terms.

Thus, for the purposes of control system design the vehicle was modelled as two uncoupled linear single-input, single-output (SISO) systems with identical double-integrator dynamics from thruster duty cycle  $r$  (from -1 to +1, corresponding to full activation of the negative or positive thrusters respectively) to angle  $\theta$  (in radians):

$$\ddot{\theta} = \frac{T_{full} r}{J}$$

$$\Rightarrow TF_{r \rightarrow \theta} = \frac{T_{full}}{J s^2}$$

The nominal moment of inertia about each axis is  $6.4 \times 10^{-3} \text{ kg m}^2$  (from the CAD model), with an assumed thruster torque of 0.2Nm at 100% duty cycle. Estimated variations in these values and thus in the overall gain are indicated in Table 5.

Parameter	Nominal	Maximum estimate	Minimum estimate
Moment of inertia, J (kg m <sup>2</sup> )	$6.4 \times 10^{-3}$	$7.7 \times 10^{-3}$	$5.1 \times 10^{-3}$
Fully-activated thruster torque, T <sub>full</sub> (Nm)	0.2	0.3	0.15
Overall gain, T <sub>full</sub> /J	40.8	76.9	25.4

Table 5: Nominal values and ranges for the dynamic properties of the vehicle. The range in the moment of inertia was determined as the nominal value  $\pm 20\%$ ; for the thruster torque, the thrust from the nozzle had been measured to be between 0.75N and 1.5N depending on test conditions, while the moment arm remained 0.2m.

## 6.2 Rate gyro sensor inputs

The ADIS16250 rate gyros used [25] have built-in analogue-to-digital converters (ADC) and are factory-calibrated to give an output in degrees per second. However, due to variations in temperature (and other factors) the analogue voltage output from the sensing portion of the device when at rest varied over time; thus the manufacturer's recommended procedure for resetting the null point was followed every time the avionics system was powered up.

To obtain estimated orientation measurements around each axis, the angular velocity reading from each rate gyro is sampled at the frequency of the control loop (see section 6.3) and integrated numerically. The rate gyros have a default analogue bandwidth of 50Hz, as well as a digital Bartlett window FIR filter with an adjustable cut-off frequency; the latter was set to 32 taps, giving a cut-off at approximately 10Hz, to prevent aliasing.

## 6.3 Control law

The approach and terminology in this section is taken from [28].

A double-integrator system, such as the transfer function from torque to angle

in a rocket in free flight, has a constant phase of  $-180^\circ$  at all frequencies. To stabilise such a system, one approach involves the use of a lead compensator – a low-frequency zero and a high-frequency pole straddling the crossover frequency – to give a good phase margin at crossover without requiring high gain at any frequency.

The settling time for the controlled system  $T_s$  (with a 2% criterion) was set at 1s with a damping coefficient  $\zeta$  of 0.45. This gives a continuous-time control law as follows:

$$G_c(s) = \frac{0.442s + 0.2528}{0.02999s + 1}$$

The frequency of the zero is 0.91Hz and that of the pole is 5.30Hz.

The continuous-time control law thus determined was then transformed to discrete time using Tustin's bilinear transformation. A sample frequency of 20Hz was chosen in order to lie intermediate between the 0dB frequency of the closed-loop system and the 50Hz PWM frequency of the valves. The discrete-time control law was implemented in state-space form with a one-dimensional state  $x$  as follows:

$$\begin{aligned} x_{n+1} &= 0.0908x_n + 2\theta_n \\ r_n &= -3.0269x_n + 9.1865\theta_n \end{aligned}$$

Bode frequency response plots of the plant transfer function, continuous-time control law, discrete-time control law and the closed-loop transfer function are shown in Figure 14.

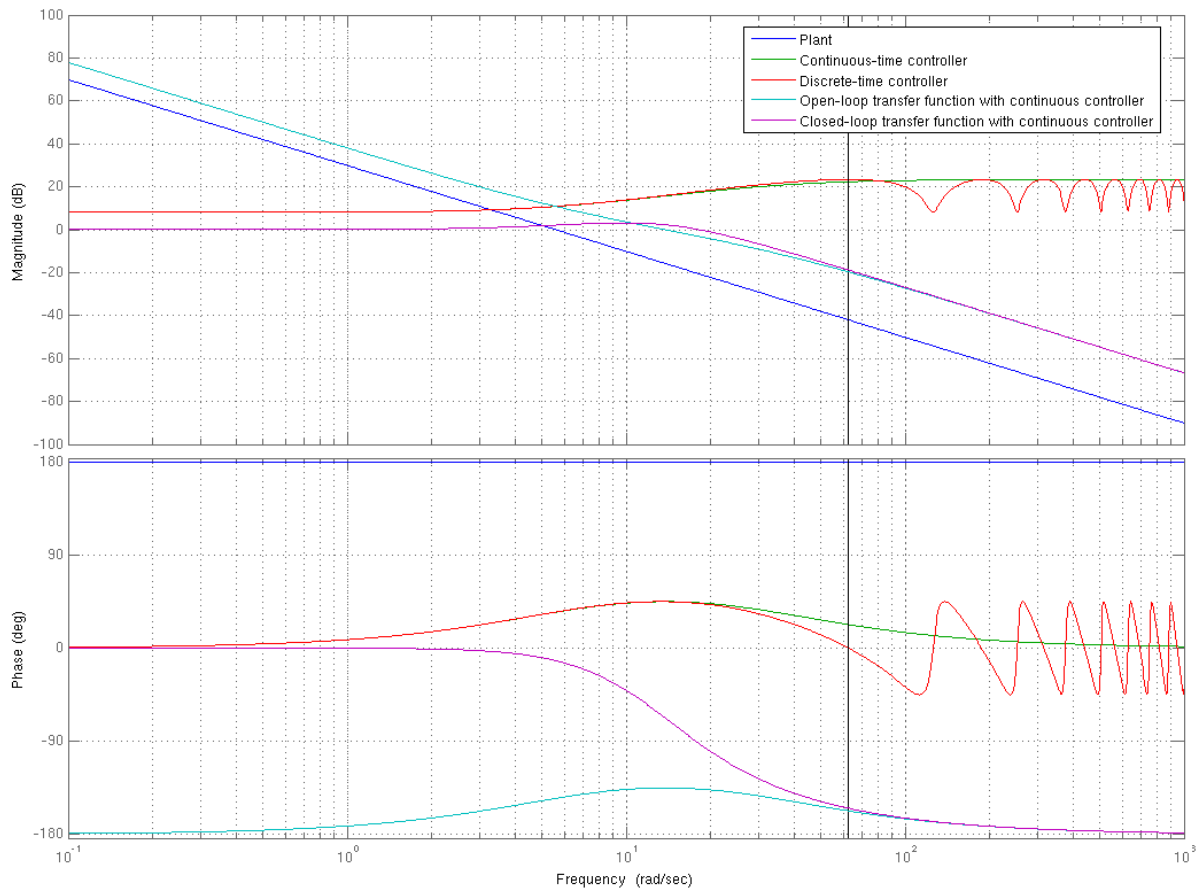


Figure 14: Bode plots of the plant, continuous and discrete-time control laws and the open- and closed-loop transfer functions. Thanks to the addition of the phase lead compensator described above, the plant is stabilised with a phase margin of  $45^\circ$  at a crossover frequency of  $13.8\text{rad/s}^{-1}$  (2.19Hz).

## 6.4 Simulation

To determine whether the stability of the system would be affected by the saturation nonlinearity due to the finite available thruster torque and the PWM frequency of the valves, numerical simulations of the control system were carried out using Matlab and Simulink software produced by The Mathworks [29]. The relevant block diagrams are shown in Figure 15 and a time-history of a simulation involving both a static disturbance torque (due to thrust vector misalignment) and random fluctuating disturbances is shown in Figure 16. This simulation predicts that the controller described above would stabilise the system even in the face of nonlinearities and disturbances.

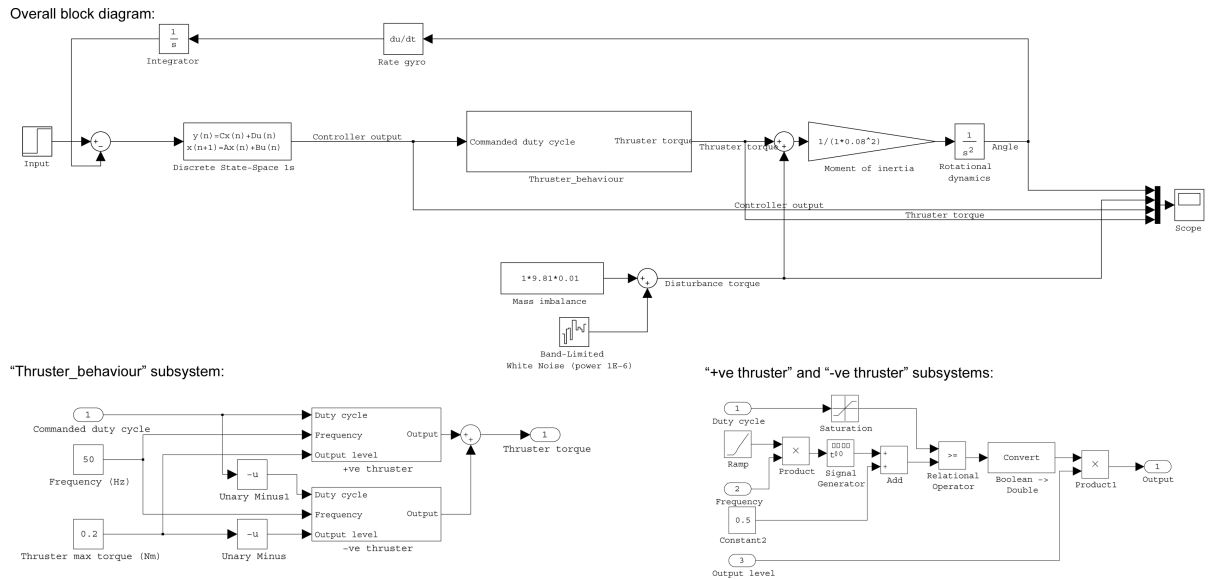


Figure 15: The Simulink block diagram used to simulate the behaviour of the system with nonlinearities from actuator saturation and PWM thruster activity. For simplicity, the mapping from controller output to thruster behaviour was encased within a subsystem and further divided into two PWM generators and appropriate interconnections. Disturbance torques acting on the vehicle include a 1cm misalignment between the thrust vector (significantly greater than expected) and the centre of mass and a fluctuating torque to model wind loading.

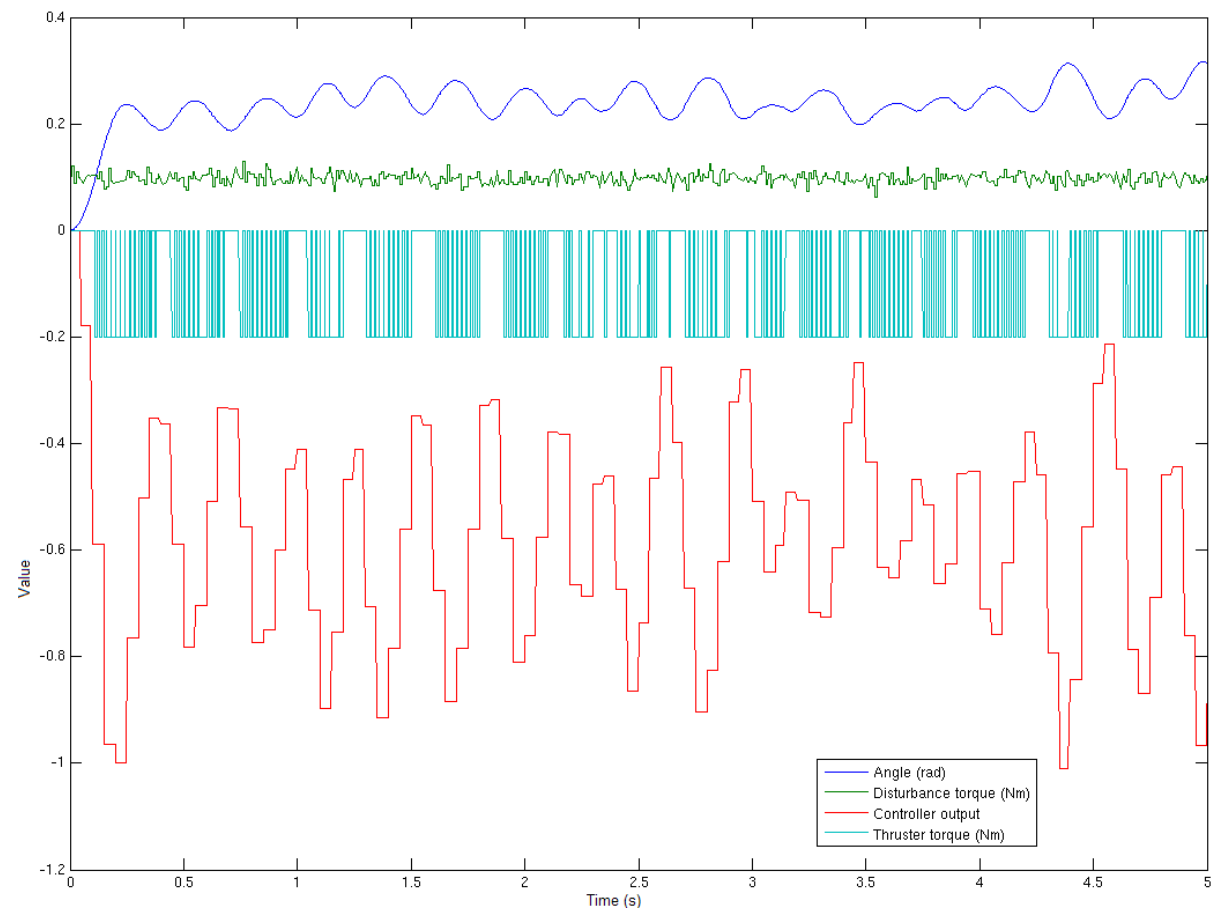


Figure 16: A simulation of the behaviour of the nonlinear system under the influence of the disturbances in the block diagram above, while attempting to maintain an attitude of  $0^\circ$ . It is observed that the actual angle fluctuates around  $0.2\text{rad}$  ( $11.5^\circ$ ) with a frequency of approximately 2Hz and an amplitude of up to  $0.1\text{rad}$  ( $6^\circ$ ) peak-to-peak; this would not be a problem for the rocket, especially since the disturbance conditions are likely to be overly harsh.

## 6.5 Software structure

The controller described above was implemented on the rocket's onboard LPC2138 processor. Overall the flight control software consists of several components:

- Launch sequencer: this waits until the rocket has been placed on the pad (i.e. until the launch detect switches are closed); it then resets the rate gyros' zero point and configures the digital filter, activates a warning buzzer and waits for one of the launch detect switches to open. Once this occurs, execution switches to the:
- Control law/datalogger loop: this is executed at a preset frequency. In each execution of the loop, the current angular velocity readings are read from the rate gyros; these are integrated to update the estimated orientation of the vehicle; and the control law is applied to derive duty cycle commands for the thrusters.
- Low-level peripheral driver functions: these allow the high-level functions mentioned above to access the processor's on-board peripherals and, through them, the sensors and actuators that form the control system. In particular, drivers were written for:
  - The processor's SPI interface
  - The functions supported by the rate gyro's digital control electronics
  - The LEDs, DIP switches and buzzer on the avionics board
  - The processor's PWM outputs

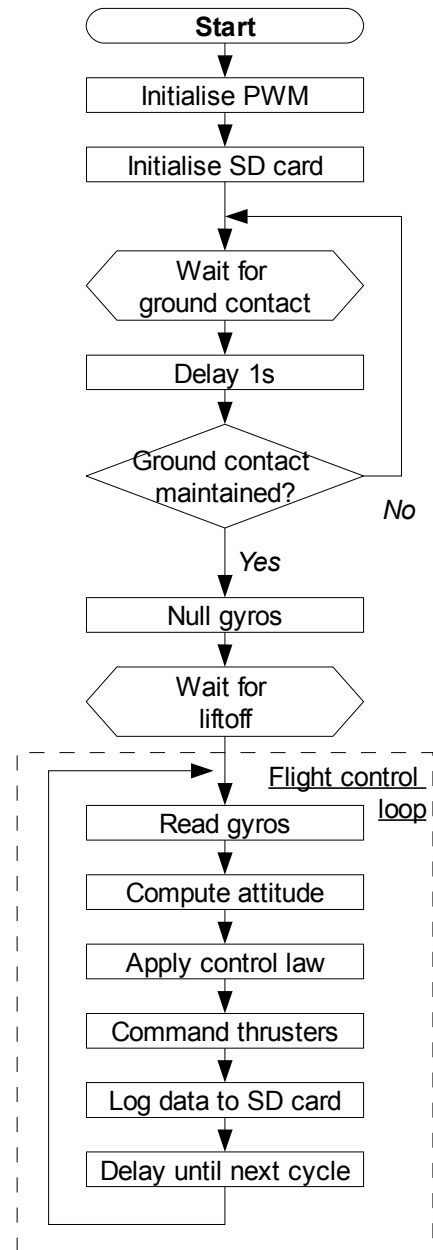


Figure 17: A flowchart showing the sequence of software states during a launch attempt. The LEDs are used to indicate the success or failure of stages in this sequence, and an audible alarm sounds to indicate the vehicle is waiting for liftoff or executing the control loop.

- The processor's analogue inputs
- The processor's built-in timers

The interface to the SD card for datalogging purposes made use of code from [30].

A flowchart illustrating the sequence of software states during a launch is shown in Figure 17.

## **6.6 Development environment and toolchain**

The manufacturer of the processor board [21] provided a development environment for the processor. Programs were written in the high-level C language on a Windows PC, compiled with the GNU C cross-compiler for ARM processors [31] and downloaded to the processor's built-in flash memory over an RS232 connection. The same RS232 connection was the primary means of testing and debugging the code.

# **7 Construction and testing**

## **7.1 Time and expenditure**

A comparison of the projected schedule (as of January 2007) and the actual schedule is shown in Figure 18. Construction of the vehicle took significantly longer than anticipated, due to over-optimistic estimation of the extent of the practical work to be carried out. As a result of this, the Phase 2 airframe design was modified to function as either a benchtop test model or a flying vehicle with minimal modification, eliminating much of the work associated with Phase 3. It was thus a simple matter to switch between bench tests with offboard power and compressed air supplies and an onboard gas supply and battery for final testing and launch.

Few specific setbacks were encountered; the principal ones were initial difficulty in obtaining key components, leading to a late start on construction, and the need for repairs after the first test flight (see section 7.6 below).

The approximate total cost of the materials and parts used in the project was £1120, of which £60 was in the form of carbon dioxide cartridges donated by

Catering & Leisure Supplies Ltd and the remainder was generously contributed by Microsoft Research.

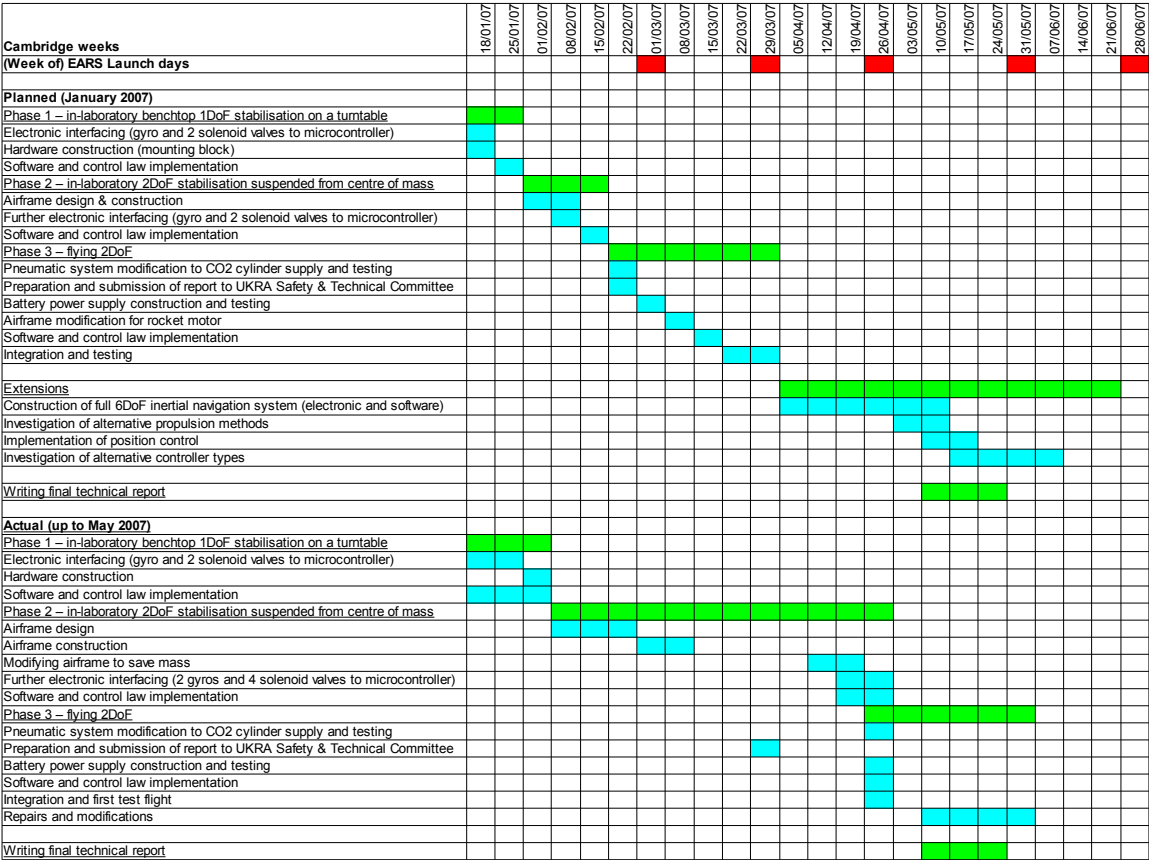


Figure 18: Gantt chart for the project, showing breakdown into Phases 1-3 and extensions.

### 7.2 Phase 1: Turntable testbed

A single-axis test rig was built to test the feasibility of the concept of cold gas jets for attitude stabilisation. This took the form of a turntable with a ball-bearing pivot, bearing a pair of solenoid valves (the Festo MHE3 model was used for this experiment) and thruster nozzles connected to the laboratory compressed air supply, a single rate gyro with its sensitive axis vertical and the processor module on the supplied development board; the apparatus is depicted in Figure 19. A manually tuned PID controller was able to demonstrate stabilisation of the turntable's angle and rejection of disturbances, as shown in Figure 20.

The concept was thus considered to be validated, and design and construction of the vehicle proceeded.

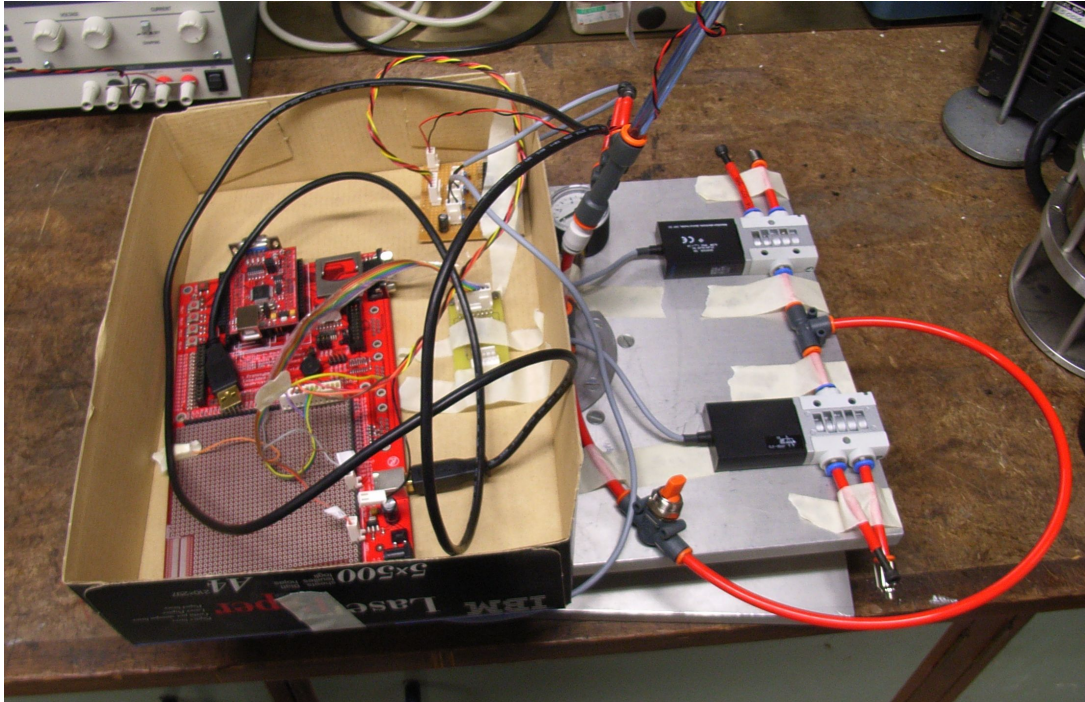


Figure 19: The turntable testbed. The aluminium turntable (27cm x 36cm) supports a cardboard box on its left side containing the processor module on its development board (at left, in red), the small yellow gyro carrier board and a circuit board with power transistors to allow the processor to control the solenoid valves. The right half of the turntable supports the two solenoid valves with attached thruster nozzles, connected to the workshop compressed air supply via the red pneumatic hoses and the blue hose at the top of the frame. Power is also supplied from offboard, via the red and black wires wound around the blue hose.

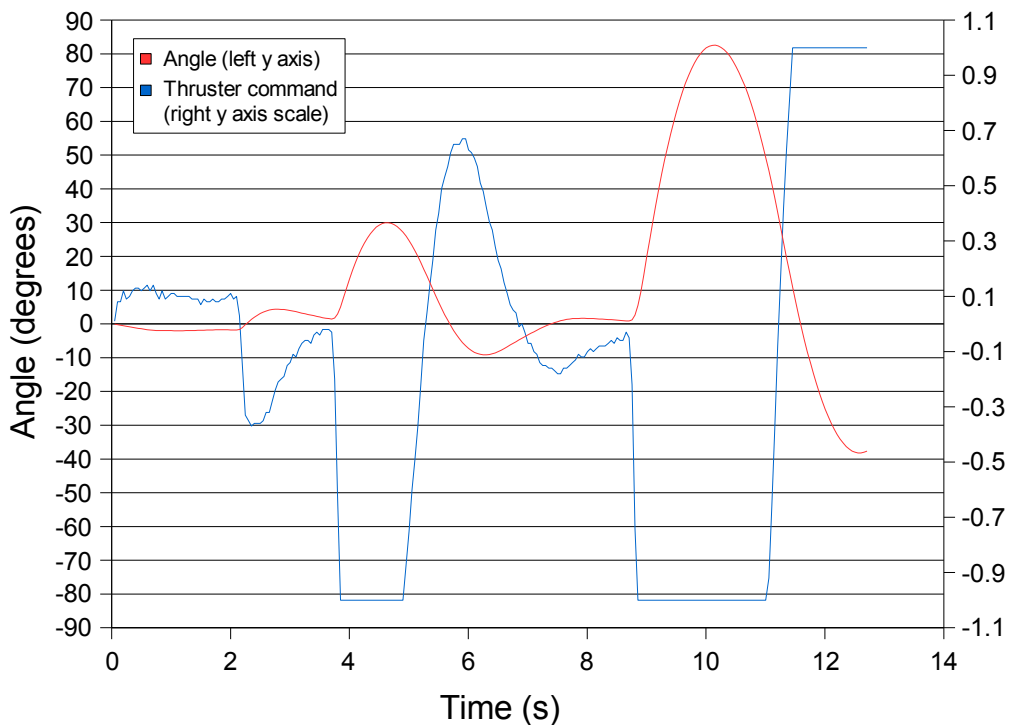


Figure 20: A trace of the angle of the turntable (as integrated from rate gyro readings, on the left hand vertical axis) and the corresponding thruster duty cycle commands (on the right hand vertical axis) against time, using a manually tuned PID controller. Impulsive disturbances were delivered to the turntable at  $t=2s$ ,  $4s$  and  $9s$  (approximately). The initial thruster activity up to  $t=2s$  was due to torsion of the air supply hose imparting a disturbance torque to the turntable. The maximum observed angular acceleration of the turntable as a result of thruster activity was  $128\text{deg/s}^2$ .

### **7.3 Phase 2 & 3 airframe construction**

The construction of the rocket took place over the period February – May 2007.

Components were sourced and fabricated as follows:

- Solenoid valves were supplied by Cambridgeshire Hydraulics and Pneumatics Ltd. and West Group UK plc ([32]).
- Pneumatic and electronic components and mechanical fasteners were supplied by Farnell UK ([33]) and RS Components Ltd ([34]).
- The processor board was supplied by Embedded Artists AB ([21]).
- The rate gyros were supplied by Arrow Electronics (UK) Ltd ([35]).
- Compressed gas cylinders and fittings were donated by Catering & Leisure Supplies Ltd ([15]) and supplied by Wiggle Ltd ([36]).
- GFRP and CFRP rod was supplied by Air Born Kites Ltd ([37]) and Active Toys ([38]).
- Rocket motor mounts were supplied by Hesperis Technology Ltd ([39]).
- Lithium polymer batteries were supplied by SkyLine Models ([40]).
- The plastic electronics housing was supplied by J Sainsbury plc ([41]).
- Four thruster nozzles, and a pivot and dummy motor for bench testing of the attitude control system, were fabricated by Mechanics Lab technicians.
- The panels for the central aluminium frame were fabricated in the Instrument Workshop using a CNC abrasivejet machining centre.
- Printed circuit boards were produced by the Electronics Development Group. Assembly was carried out in the Mechanics Mezzanine Lab and the Instrument

Workshop.

A photograph of the assembled Phase 2 & 3 airframe is shown in Figure 21.

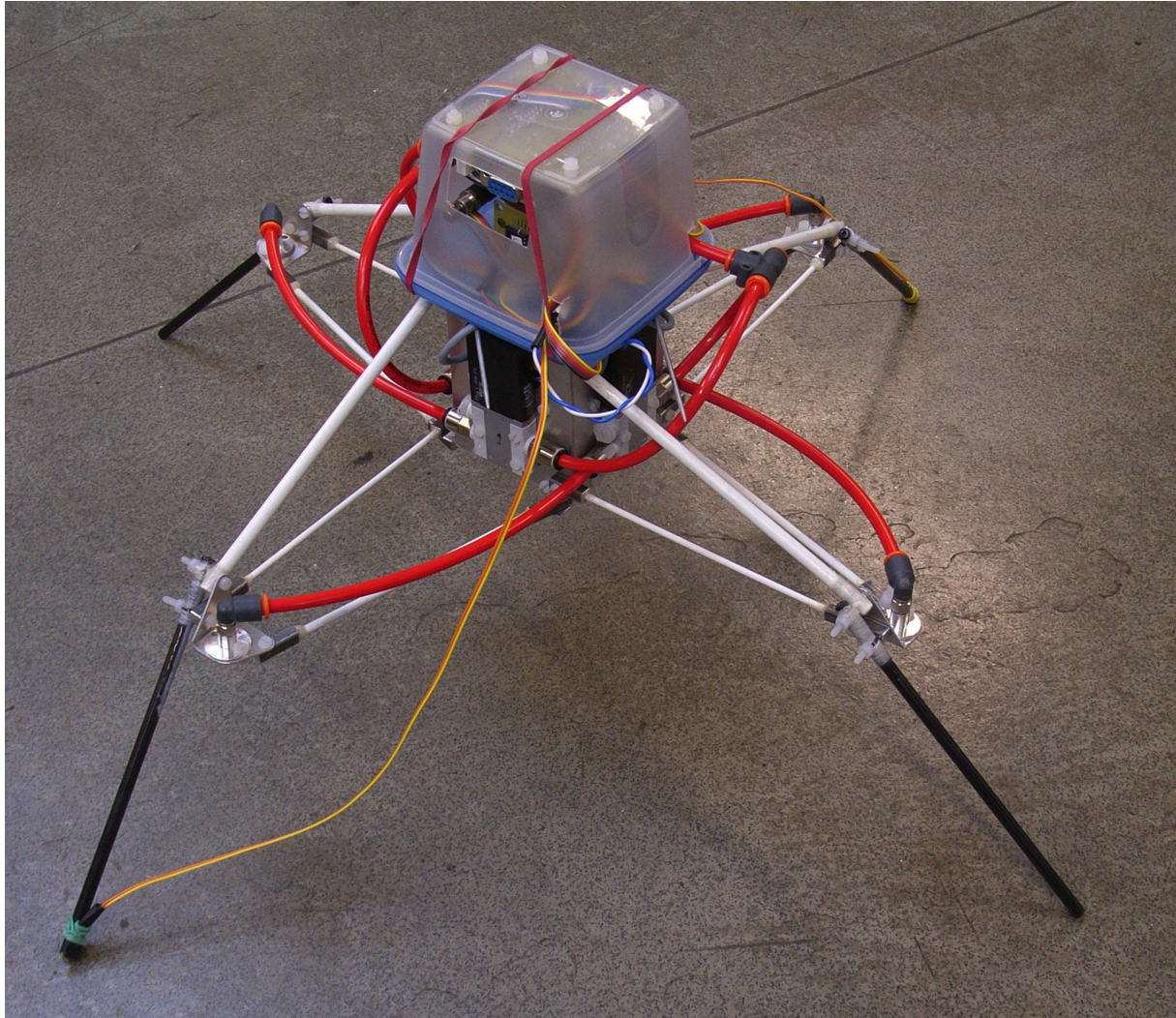


Figure 21: The Phase 2 & 3 airframe, "Kestrel". The central aluminium box houses the rocket motor, batteries and gas supply; the solenoid valves are mounted to the outside, as are the proximal ends of the primary trusses. Each primary truss holds a thruster nozzle at its tip (identifiable by the red pneumatic hose and grey pneumatic fitting attached to it), as well as a landing leg. The plastic housing on top contains the main avionics board and the gyros (the latter mounted via a bracket to the airframe), as well as the gas cylinder fitting, pressure regulator and cabling. The valve driver board is in the lower part of the aluminium frame.

## 7.4 Mass reduction

The predicted mass of the mechanical parts of the airframe, based on the CAD model of the rocket, was 700g (which would give an overall rocket mass of 1kg); however, after Phase 2 & 3 construction its mass was found to exceed this value by around 300g. To reduce the mass to the appropriate value a number of methods were used, notably:

- Replacing steel fasteners with commercial and custom-made nylon equivalents (saving: 90g)
- Removing aluminium endcaps on truss segments (saving: 53g)

- Substituting the gas cylinder adapter for a lighter equivalent, modified with a custom-made outlet port to fit directly to the downstream pneumatic components (saving: 40g)
- Removing parts of the central aluminium box frame that did not contribute to structural strength (saving: 22g)

## **7.5 Bench tests**

One of the unusual aspects of attitude thrusters compared with other methods of active stabilisation is that the control system is entirely decoupled from the rocket motor. Full advantage was taken of this to allow the control system to be tested on a bench, with the task of balancing on a pivot (a steel spike in a conical aluminium socket) placed in the motor mount, close to the vehicle's centre of mass.

Such testing was performed multiple times during integration of the vehicle; initially all the avionics were off-board, but as components were constructed they were attached in place onboard the airframe. It was also invaluable in identifying crucial bugs in the flight control software. A photograph of an early-stage bench test is shown in Figure 22; later bench tests integrated more of the components onto the vehicle, and used onboard gas cylinders rather than offboard compressed air due to the disturbance torque, spring constant and damping produced by the pneumatic hose.

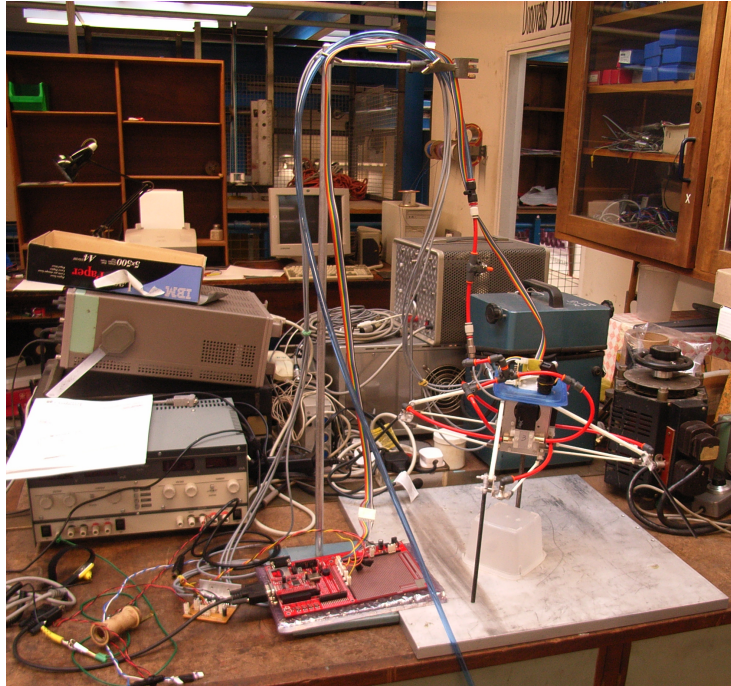


*Figure 22: Bench testing of the airframe and control system. In this image the processor, power supply and air supply are all off-board (at left), attached via an umbilical supported by the retort stand; the spike is visible underneath the airframe. Such an early-stage bench test was not used for trialling control laws but for integrating and testing the various pneumatics and avionics components.*

Perhaps most importantly, bench testing allowed the testing of control laws without the issues associated with the use of rocket motors. This system, with the dynamics of a short pendulum, approximates the real system (with double-integrator dynamics).

However, when tested with the control law derived in section 6.3, the airframe was observed to oscillate unstably even at reduced pneumatic system pressures (corresponding to reduced overall gain, which should serve to mitigate instabilities). A sample time history from such a bench test is shown in Figure 23, showing clearly the increasing amplitude of oscillations until a limit cycle is reached. It is notable that actuator saturation is not reached on either axis, implying that the thruster nonlinearity is not to blame for this oscillation (bearing out the results of the numerical simulation described in section 6.4); instead, other unmodelled dynamics of the system must be causing the oscillation. One obvious explanation is coupling between the rotation axes, shown by the synchronisation of oscillations between the two axes. This was neglected in the system model but may have arisen through one or more of:

- Misalignment of the gyro sensitive axes
- Misalignment of thrusters
- Off-diagonal terms in the moment of inertia tensor

Further investigation is necessary to determine the cause and to implement an appropriate multi-input multi-output (MIMO) control law.

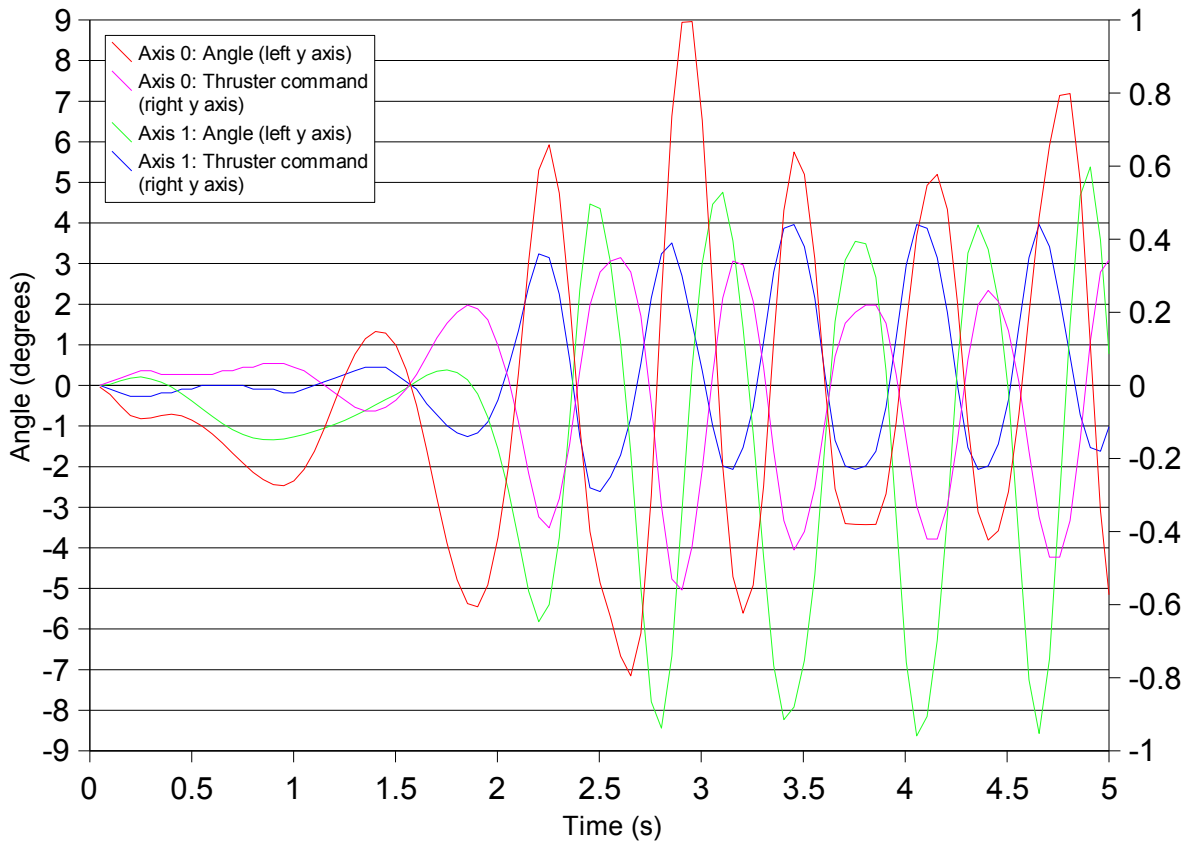


Figure 23: Logged data from a bench test using an onboard gas cylinder with a dual SISO lead controller. The angles about axis 0 and 1 are plotted against the left hand y axis, the thruster duty cycle commands on the right axis.

## 7.6 Maiden flight

Although the control system was not fully functional, as described above, it was decided to take the opportunity to test-launch the vehicle, named “Kestrel”, to gain experience of the phenomena that might be expected in flight. This took place at the East Anglian Rocketry Society (EARS) [11] “Big EARS” launch event near Elsworth, Cambridgeshire, on 6 May 2007. The vehicle was launched on an Estes E9-P motor from a flat aluminium baseplate (with no launch guides) in a sheltered area to minimise wind effects.

The audible alarm was heard before launch, showing that the launch sequencer

routine was active and waiting for launch detection, but on liftoff the rocket rapidly veered away from the vertical and crashed into the ground nearby within 1 second of ignition. A sequence of photographs of the launch is shown in Figure 24.

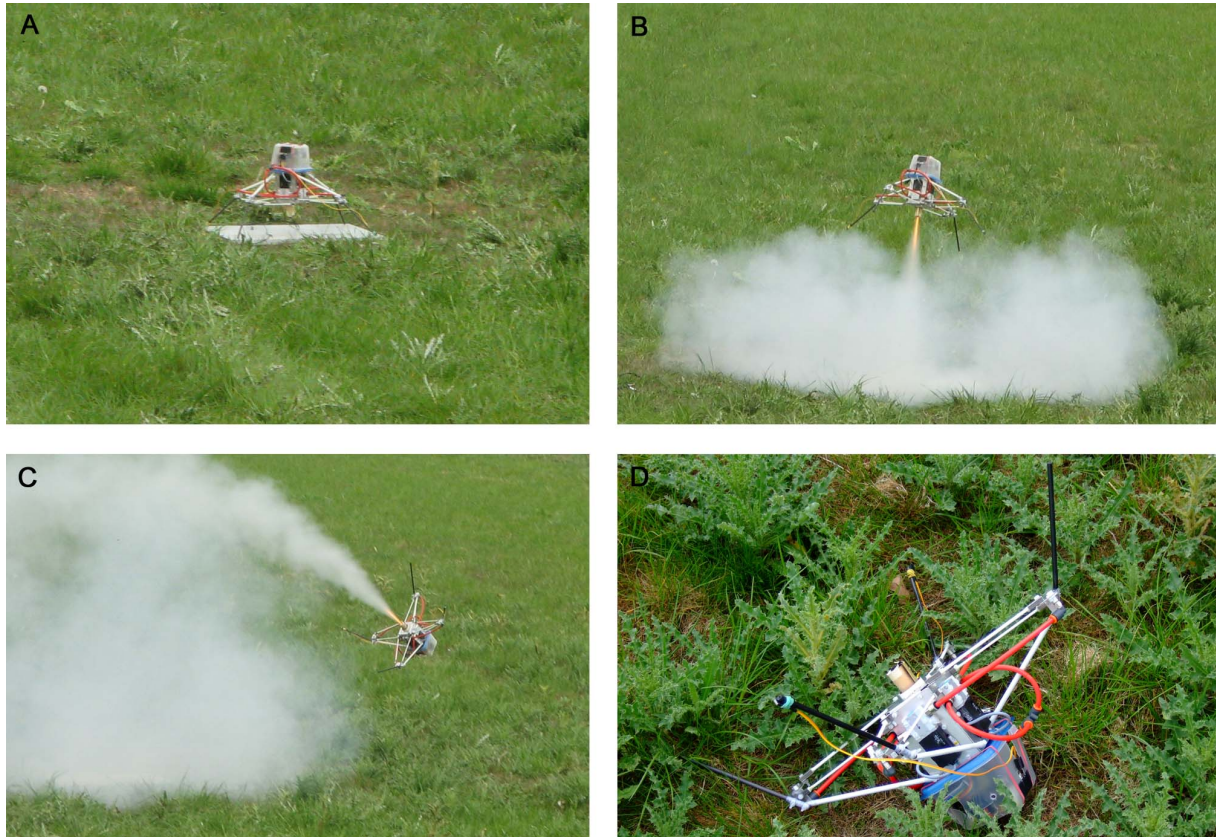


Figure 24: The launch of the rocket. A: The rocket on the launch pad. B: Shortly after liftoff the rocket begins to veer off course. C: The rocket continues rotating and after reaching a height of about 0.5m turns back towards the ground. D: The rocket as it landed. (Photographs: A,B,C: Kane Chandler; D: Ed Moore)

Due to the malfunction the rocket crashed upside down, with the electronics housing hitting the ground first. Such a failure mode had not been anticipated, meaning that the electronics housing was not designed to resist the impact; the housing fractured and damage was caused to the processor board and one of the gyro boards. As well as requiring repair, this and the fact that the datalogging function had not been integrated into the flight control software meant it was not possible to ascertain whether the control law loop had been active during the flight or what its outputs were. Evidence relevant to establishing the cause of the failure includes:

- In previous bench tests, following the audible alarm and simulation of launch (by releasing the ground contact switches) the flight controller had always

been activated.

- A drop in supply voltage to the processor during the flight would reset the control software, returning it to the “Wait for ground contact” state.
- Experienced observers noted that the behaviour of the vehicle in flight resembled that of incorrectly-built model rockets with low or zero passive stability margin.
- A slow gas leak could be heard for a number of minutes after the flight. This suggests that a substantial quantity of carbon dioxide remained in the cylinder; since bench tests indicated that a cylinder was emptied after a few seconds when the control law was active, it is likely that the solenoid valves did not operate significantly.
- No observers reported hearing the loud buzz associated with operation of the solenoid valves or seeing disturbances of the smoke plume from the motor that could be ascribed to the thrusters' exhaust; however, it is not certain whether either of these effects would have been observable under the circumstances of the launch.
- It was later discovered that a software fault had meant that a different control law from that intended had been active; this incorrect control law had been shown to have a definite effect on the rocket's dynamics in bench tests, although it was not fully stabilising.

The balance of evidence suggests that the flight control loop was not triggered (possibly due to a transient voltage drop resetting the processor) and thus the vehicle behaved as an inert mass under the influence of the rocket motor's thrust and gravity.

Positive outcomes from the test flight included experience gained with launching the vehicle using rocket motors and the highlighting of a number of issues with the rocket's design to improve:

- The importance of a means of measuring hidden state of a control system in order to find out the cause of a failure was highlighted. A datalogger interface was integrated into the flight control software with the highest priority.

- The screws securing the top plate of the central aluminium frame, which had to be removed to access and replace the gas cylinder and batteries, were very difficult and fiddly to remove. This made it time-consuming to replace the gas cylinder between tests, and meant that the batteries could not be removed quickly to make the rocket safe. These were replaced by metal pins that could be inserted and removed rapidly.
- Visual or audible confirmation that the processor is operational and the program is running was implemented using the onboard LEDs to signal the state of the launch sequencer.
- It is important to protect the electronics housing better in case of major malfunction – for example using “roll bars”. This consideration will be taken into account before the next flight test.

## **8 Conclusions**

### **8.1 Project achievements and validity of concept**

An attitude thruster stabilisation system for a small rocket was designed and constructed using mostly commercially-available components, for a cost of around £1120. Funding to pursue the project was contributed by Microsoft Research.

Numerical simulations indicated that the control system would stabilise and control the vehicle appropriately. However, bench tests of the real system's dynamics (made possible by the initial choice of an attitude control system that was independent of the rocket motor) showed instability; it is suspected that this is due to cross-axis coupling that was neglected during controller design.

A trial launch was conducted to gain experience and test the control system in flight. The test did not appear to show any control activity, possibly due to resetting of the processor at the instant of launch.

Although the project has not yet demonstrated a stabilising control system, the underlying hardware and software functions correctly and in principle the aim could be achieved by appropriate redesign of the control law facilitated by bench testing on the real system. It is hoped that development will continue and future test flights will

be able to show a fully functioning attitude control system.

## **8.2 Project significance**

One of the aims of this project was to develop an active stabilisation system that could be applied to more conventional amateur rockets to control the ascent trajectory despite cross-winds and other disturbances. It was conjectured at the conceptual design stage that attitude thrusters were not the most applicable method in this regard, due to the considerable additional mass and volume they occupy, but they were chosen for their suitability in other respects (ease of design and construction as well as independence from the rocket motor).

This is vindicated by the experience of constructing the vehicle “Kestrel”. Adding the hardware of the control system to a conventional rocket would likely outweigh the benefits of active stabilisation, especially given the mass of the gas supply needed for a longer flight and/or higher thrust levels. A control system such as this one would likely be of most value in a low-velocity rocket where aerodynamic stabilisation (active or passive) is ineffective and manipulating the direction of the rocket exhaust is not practical; this is very similar to the situation of orbiting space vehicles where attitude thrusters are commonly used.

Nonetheless, the attitude determination and computational hardware and software developed for this project could well be used to control other types of actuators for attitude stabilisation systems. It would be particularly straightforward to adapt the software to control conventional hobby servos, since they are also controlled by pulse-width-modulation signals ([42]).

## **8.3 Evaluation of approach**

- The construction of the vehicle required significantly more time than given in the initial plan. This was due to over-optimistic estimation of the time required for practical tasks and neglecting to consider design iteration, rework etc.
- The importance of a means of measuring hidden state during tests in order to find out the cause of a failure was highlighted by its lack in the first flight of

the vehicle.

- At several points, models of the vehicle's dynamics were used that were later found to be inaccurate – both mathematical models that neglected important dynamics (e.g. cross-axis coupling) and physical test setups that have external disturbances (e.g. forces from umbilical connections). It is important to recognise for what purposes a given model is sufficiently faithful and when it is appropriate to switch to a more complex and accurate model.
- The choice of a stabilisation concept that could easily be tested under laboratory conditions aided system-level integration considerably compared with a concept that could only be tested in flight.
- During integration, problems with subsystems were frequently resolved successfully by a methodical reductionist approach of testing the functioning of every component in isolation prior to integration.
- When undertaking field work, it was found to be difficult to predict which items of equipment would be necessary under a given set of circumstances; thus, as many items as practical should be kept to hand.

## 8.4 Future work

As noted above, in order to achieve the aims of this project the control law should be redesigned using an approach that considers the true multi-input multi-output (MIMO) dynamics of the vehicle - for example, MIMO pole placement or  $H_\infty$ -optimal controller synthesis (described in [43]). The latter method can be used to give a control law that is guaranteed to be robust against variations in the plant parameters up to a certain level. Some modifications to the airframe (particularly the electronics housing) could also be made to increase its physical robustness to impact.

Following this, a number of enhancements could be made to the vehicle to enhance its capabilities. These include:

- Extended flight duration: By using a more powerful motor (e.g. the Aerotech G12-RCT ([14])) and a larger gas cylinder, the duration of the flight might be extended from 3s to 9s.
- Position control: By controlling the vehicle's attitude, the actuators give

indirect control over position in a horizontal plane. In order to implement this, sensors would be required to measure the vehicle's attitude in all 6 degrees of freedom (DoF) – for example, an extra rate gyro and three orthogonal accelerometers – and an additional pair of thrusters would be necessary to control the roll axis.

- Onboard autonomy: The vehicle could be equipped with sensors to allow it to execute simple tasks while airborne (e.g. following a white line).

## 9 Acknowledgements

I would like to thank my supervisors, Dr Hugh Hunt (CUED) and Professor Chris Bishop (Microsoft Research), for providing resources, advice and assistance throughout the course of the project. I am particularly grateful to Microsoft Research for contributing the majority of the funding for this project.

I would also like to thank the numerous other people who have helped me with the design and construction of the rocket, in particular:

- Gary Bailey (CUED)
- Simon Box (Microsoft Research)
- Kane Chandler
- Caizen Cheng (CUED)
- Richard Christmas (CUED)
- Marco Costanzi (CUED)
- Helen Craig
- Jason Crick (Cambridgeshire Hydraulics and Pneumatics)
- Damian Hall (EARS)
- Henry Hallam
- Andy Hughes (Silicon Sensing)
- Peter Long (CUED)
- Jim Macfarlane (EARS)
- Rob Macfarlane
- David Miller (CUED)
- Jon Money (Catering & Leisure Supplies Ltd)
- Ed Moore
- Brendan O'Donoghue
- Mike Roberts (EARS)
- Alastair Ross (CUED)
- Jeremy & Sylvia Wyatt

## 10 References

- [1] "Active Guidance", <http://www.ukrocketman.com/rocketry/gimbal.shtml> (accessed 15/01/2007)
- [2] "Studio di veicolo con stabilizzazione attiva", <http://www.criscaso.com/razzimodellismo/Casimiro/> (accessed 15/01/2007)
- [3] NASA, 2004: "The Vision for Space Exploration" (accessed via [http://www.nasa.gov/pdf/55583main\\_vision\\_space\\_exploration2.pdf](http://www.nasa.gov/pdf/55583main_vision_space_exploration2.pdf))
- [4] "NASA Centennial Challenges", [http://exploration.nasa.gov/centennialchallenge/cc\\_challenges.html](http://exploration.nasa.gov/centennialchallenge/cc_challenges.html) (accessed 15/01/2007)
- [5] "Martlet", <http://www.cuspaceflight.co.uk/martlet.html> (15/01/2007)
- [6] Cambridge University Engineering Department, 2003: "Properties of the International Standard Atmosphere at Altitude", in Thermofluids Data Book
- [7] Cornelisse J W, Schöeyer H F R, Wakker K F, 1979: "Rocket propulsion & spaceflight dynamics" (Pitman, 1st edition)
- [8] "Murata Boy website", <http://www.murataboy.com/en/> (accessed 26/5/2007)
- [9] Freescale Semiconductor, inc, 2004: "SPI block guide" (accessed via [http://www.freescale.com/files/microcontrollers/doc/ref\\_manual/S12SPIV4.pdf?srch=1](http://www.freescale.com/files/microcontrollers/doc/ref_manual/S12SPIV4.pdf?srch=1))
- [10] UK Rocketry Association, 2004: "UKRA safety code v4.21" (accessed via [http://www.ukra.org.uk/docs/Safetycode\\_v421.pdf](http://www.ukra.org.uk/docs/Safetycode_v421.pdf))
- [11] "East Anglian Rocketry Society website", <http://www.ears.org.uk/> (accessed 15/01/2007)
- [12] "E9-P information page", <http://www.estesrockets.com/products.php?number=1676> (accessed 15/01/2007)
- [13] USA National Association of Rocketry, 2001: "Estes E9-X certification data" (accessed via <http://www.nar.org/SandT/pdf/Estes/E9.pdf>)
- [14] AeroTech Rocketry, 2005: "2005-2006 product catalogue" (accessed via [http://www.aerotech-rocketry.com/customersite/resource\\_library/Catalogs\\_Flyers\\_Data\\_Sheets/2005\\_aerotech\\_catalog.pdf](http://www.aerotech-rocketry.com/customersite/resource_library/Catalogs_Flyers_Data_Sheets/2005_aerotech_catalog.pdf))
- [15] "Tyre-Inflators.co.uk website", <http://www.tyre-inflators.co.uk/> (accessed 15/01/2007)
- [16] Vukalovich M P, Altunin V V, 1968: "Thermophysical properties of carbon dioxide" (Collet's, 1st edition)
- [17] Sidi M J, 1997: "Spacecraft Dynamics and Control" (Cambridge University Press,

1st edition)

- [18] "Festo website", <http://www.festo.com> (accessed 15/01/2007)
- [19] NXP Semiconductor, 2006: "LPC2138 Datasheet" (accessed via [http://www.nxp.com/acrobat\\_download/datasheets/LPC2131\\_32\\_34\\_36\\_38\\_3.pdf](http://www.nxp.com/acrobat_download/datasheets/LPC2131_32_34_36_38_3.pdf))
- [20] "NXP Semiconductors website", <http://www.nxp.com> (accessed 15/01/2007)
- [21] "Embedded Artists website", <http://www.embeddedartists.com> (accessed 15/01/2007)
- [22] Barbour N M, Elwell J M, Setterlund R H, 1992: "Inertial instruments - where to now?", in Proceedings of the AIAA Guidance, Navigation and Control Conference, Hilton Head Island, SC, Aug. 10-12, 1992
- [23] Apostolyuk V, 2006: "Theory and design of micromechanical vibratory gyroscopes" (accessed via <http://www.astrise.com/research/library/memsgyro.pdf>)
- [24] "Analog Devices website", <http://www.analog.com> (accessed 15/01/2007)
- [25] Analog Devices, 2007: "ADIS16250/16255 Datasheet" (accessed via [http://www.analog.com/UploadedFiles/Data\\_Sheets/ADIS16250\\_16255.pdf](http://www.analog.com/UploadedFiles/Data_Sheets/ADIS16250_16255.pdf))
- [26] Geen J, Krakauer D, 2003: "New iMEMS® Angular-Rate-Sensing Gyroscope" (Analog Dialogue 37; accessed via <http://www.analog.com/library/analogDialogue/archives/37-03/gyro.html>)
- [27] "Thunder Power website", <http://www.thunderpower-batteries.com/> (accessed 28/05/07)
- [28] Dorf R C, Bishop R H, 2005: "Modern Control Systems" (Pearson Prentice Hall, 10th edition)
- [29] "The Mathworks website", <http://www.mathworks.com> (accessed 18/05/2007)
- [30] NXP Semiconductor, 2007: "AN10406: Accessing SD/MMC card using SPI on LPC2000" (accessed via <http://www.standardics.nxp.com/support/documents/microcontrollers/pdf/an10406.pdf>)
- [31] "GNU ARM toolchain website", <http://www.gnuarm.org/> (accessed 17/05/2007)
- [32] "Cambridgeshire Hydraulics and Pneumatics website", <http://www.cambshydraulics.com/> (accessed 29/5/07)
- [33] "Farnell UK website", <http://uk.farnell.com/> (accessed 29/5/2007)
- [34] "RS Components Ltd website", <http://www.rswww.com/> (accessed 29/5/2007)
- [35] "Arrow Northern Europe website", <http://www.arrowne.com/> (accessed 29/5/2007)
- [36] "Wiggle Ltd website", <http://www.wiggle.co.uk> (accessed 29/5/2007)

- [37] "Air Born Kites Ltd website", <http://www.airbornkites.co.uk/> (accessed 29/5/2007)
- [38] "Active Toys website", <http://www.activetoys.co.uk/> (accessed 29/5/2007)
- [39] "Hesperis Technology Ltd website", <http://www.modelrockets.co.uk/> (accessed 29/5/2007)
- [40] "SkyLine Models website", <http://www.skylinemodels.co.uk/> (accessed 29/5/2007)
- [41] "J Sainsbury plc website", <http://www.sainsburys.co.uk/> (accessed 29/5/2007)
- [42] McComb G, Predko M, 2006: "The Robot Builder's Bonanza" (McGraw-Hill/TAB Electronics, 3rd edition)
- [43] Zhou K, Doyle J C, Glover K, 1996: "Robust and Optimal Control" (Prentice Hall, 1st edition)
- [44] Cambridge University Engineering Department, 2003: "Physical and Mechanical Properties of Materials", in Materials Data Book
- [45] "CadSoft website", <http://www.cadsoft.de/> (accessed 28/05/07)

## Appendix A: Structural design of primary truss and landing legs

The identifiers for the different elements of the primary truss are shown in Figure 25.

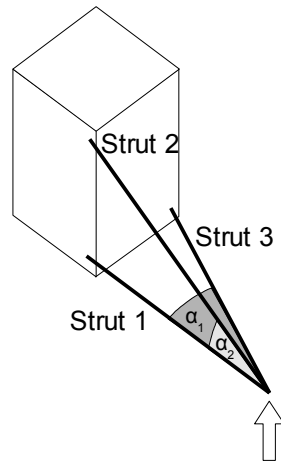


Figure 25: Components of primary truss structure

The values of the angles are:

$$\alpha_1 = 16^\circ$$

$$\alpha_2 = 21^\circ$$

The value of the landing force  $F_{L, peak}$  was calculated as follows:

$$F_{L, average} = \frac{m v_{impact}}{t_{impact}} = \frac{1\text{kg} \times 5\text{ms}^{-1}}{0.1\text{s}} = 50\text{N}$$

$$F_{L, peak} = 2F_{L, average} = 100\text{N}$$

Assuming that this is carried purely by strut 1 in tension and strut 2 in compression, using static equilibrium and pin-jointed analysis this gives:

$$T_2 = 100\text{N} / \sin(21^\circ) = -278\text{N}$$

$$T_1 = -T_2 \cos(21^\circ) = 259\text{N}$$

The struts were then sized to withstand yield failure in tension and Euler buckling in compression. Although reversible elastic Euler buckling on landing would not be problematic for the structure, it was assumed it would represent a lower limit on the failure load. The material assumed was glass fibre reinforced polymer (GFRP) kite spar of circular cross-section, with properties  $E_{\text{GFRP}} = 15\text{GPa}$  and  $\sigma_{y, \text{GFRP}} = 110\text{MPa}$  (taken from [44]). The results are shown in Table 6.

<b>Strut</b>	<b>Length (mm)</b>	<b>Load (N)</b>	<b>Minimum diameter (mm)</b>	<b>Actual diameter (mm)</b>
1	158	+259	1.7	3
2	177	-278	5.9	6.35
3	153	±50 (estimated)	3.6	4

Table 6: Sizing of primary truss struts. The "Actual diameter" column reflects the actual availability of GFRP pultrusion.

The landing legs were modelled as a tip-loaded cantilever of 150mm length and were assumed to be carbon fibre reinforced polymer (CFRP) kite spar of circular cross-section, with  $\sigma_{y, \text{CFRP}} = 750\text{MPa}$ . The design criterion was to avoid failure in yield at the root under 100N loading; this led to a minimum diameter of 5.9mm, and an actual diameter of 6mm.

## Appendix B: Thruster nozzle final design

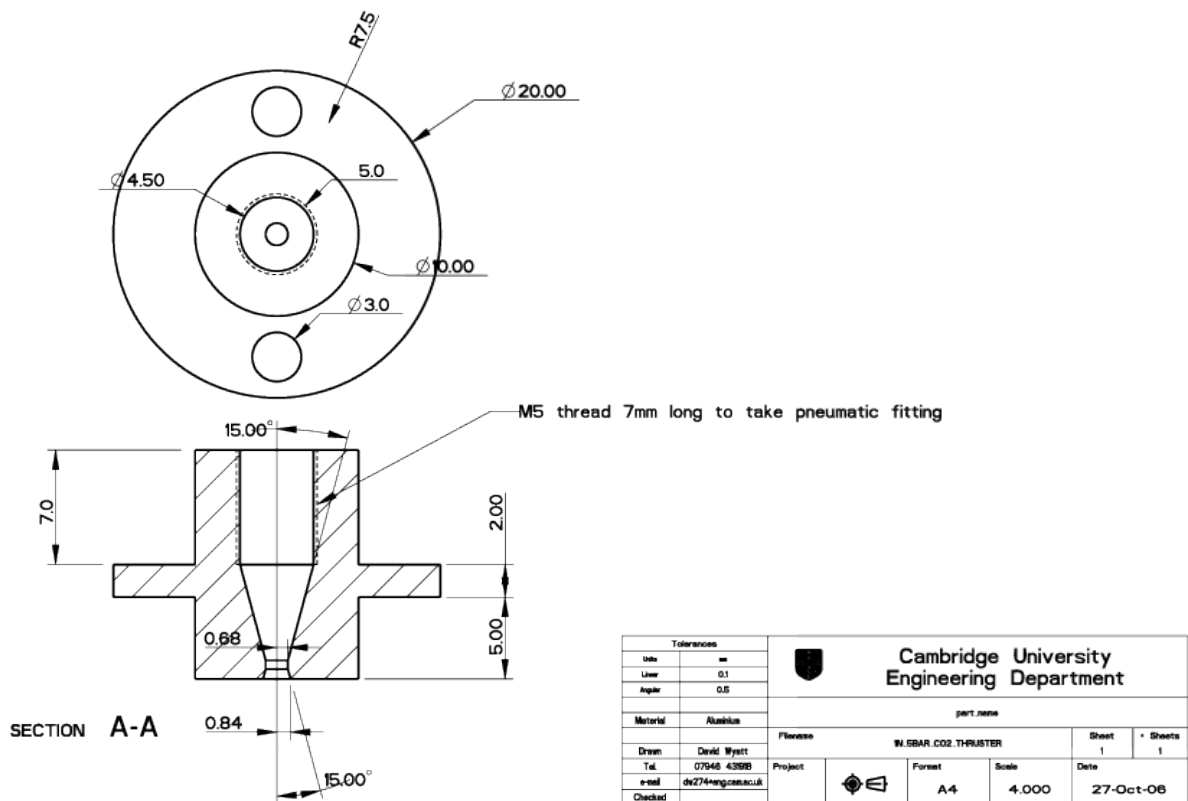


Figure 26: Design for the 1N, 5bar inlet thruster nozzle (all dimensions in mm). The M5 thread on the inlet accepts a standard pneumatic fitting; the flange and holes are for mounting to the vehicle's structure.

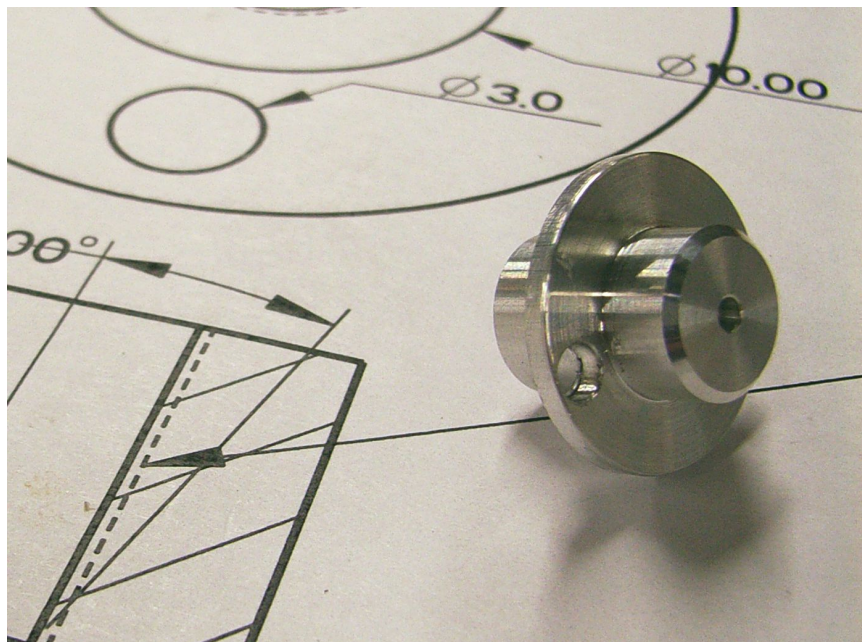


Figure 27: The prototype nozzle.

## Appendix C: Requirements for rocketry avionics

Avionics requirements for generalised rocketry projects are shown in Table 7 (compiled in collaboration with Brendan O'Donoghue).

Function	Estimated numerical specifications	Present or future need?	Processor requirement
3 orthogonal gyroscopes	Up to 300°/s each axis	2 present, 1 future	3 analogue inputs or SPI interface
6 solenoid valves	24V 1A	4 present, 2 future	6 PWM digital outputs
Arming switch		Present	1 digital input
Liftoff detector		Present	1 digital input
Non-volatile data logging	150 bytes at 50Hz	Present	Non-volatile memory or SPI interface to SD card
Real-time control	up to 100Hz control loop	Present	Fast floating-point calculations
Signalling avionics state	4 LEDs, 1 buzzer	Present	5 digital outputs
Timing	0.01ms resolution	Present	Timers
Uploading/downloading data	RS232	Present	UART
3 orthogonal accelerometers	Up to 5g each axis	Future	3 analogue inputs or SPI interface
4 radio-control servomotors	PWM, 50Hz update	Future	4 PWM digital outputs
Barometric pressure sensor	1 mBar resolution, range 0.3Bar to 2Bar	Future	1 analogue input
Kalman filtering/IMU functions	6 DoF, 12 states	Future	Fast floating-point calculations
Recovery system deployment (2 electric igniters)	20A for 200ms	Future	2 digital outputs
Wind velocity sensor (3 axes)	Up to 500m/s	Future	3 analogue inputs

Table 7: Interface and other requirements for avionics systems for rocketry projects, divided between present needs (required by this project) and future needs (potentially required by other projects).

The requirements on the processor in particular are:

- 10 analogue inputs
- Fast floating-point calculations
- (Interface to) non-volatile memory
- 11 digital outputs (6 PWM capable), 2 digital inputs
- RS232 communication
- SPI bus
- Timers

# Appendix D: Avionics circuit diagrams and circuit board layouts

All circuit diagrams and printed circuit board (PCB) layouts were produced using Eagle ECAD software from CadSoft [45] except where otherwise stated.

## Main avionics board

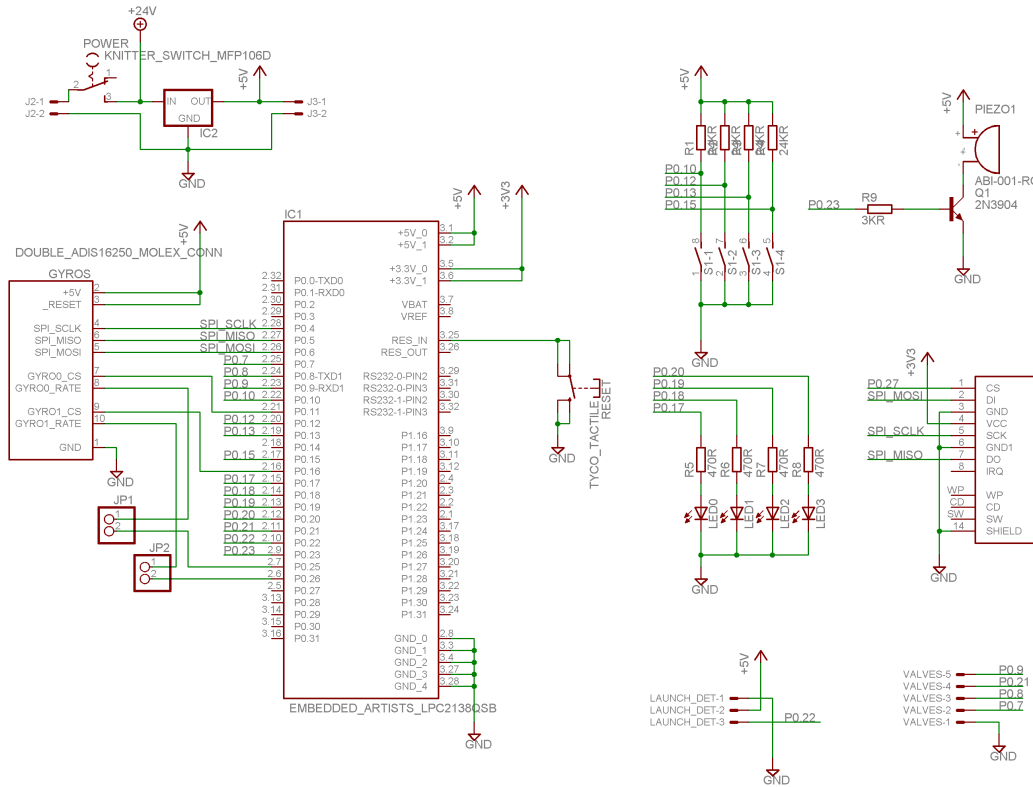


Figure 28: Schematic for the main avionics board.

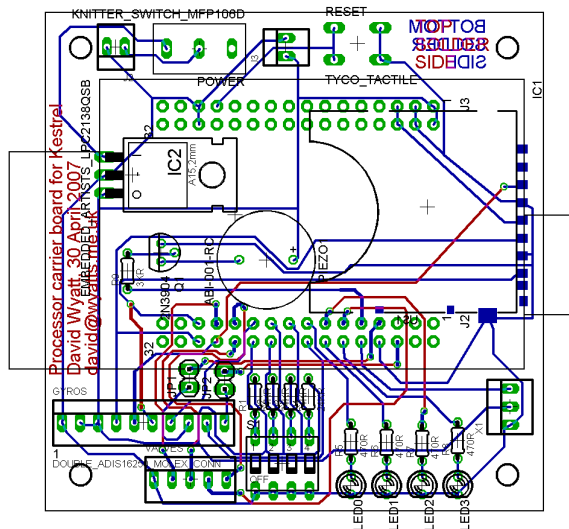


Figure 29: Printed circuit board layout for the main avionics board. This is a double-sided PCB with hand-soldered vias; red denotes traces on the top of the board, blue denotes traces on the bottom. The board is 70mm square.

## Valve driver board

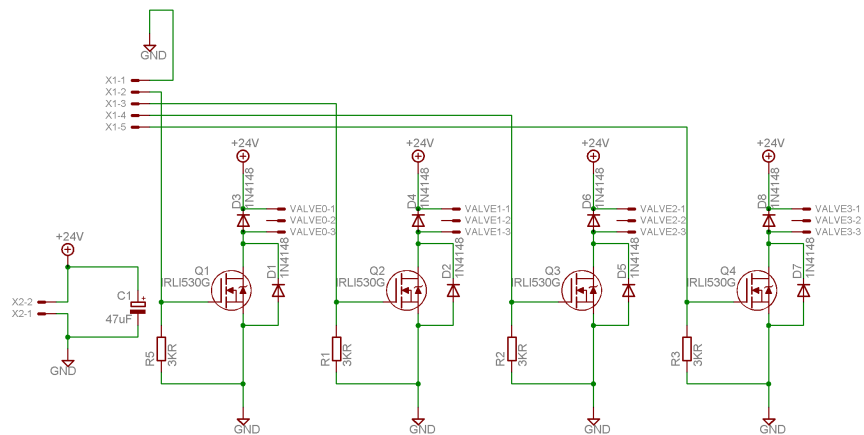


Figure 30: Schematic for the valve driver board. The original circuit for this board was designed by Gary Bailey.

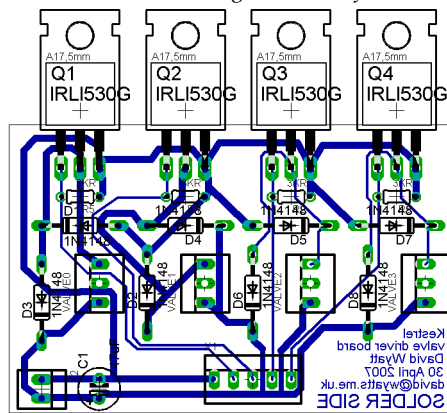


Figure 31: PCB layout for the valve driver board. This is a single-sided circuit board, 58mm x 38mm.

## Gyro board

This circuit board was purely a breakout board; the PCB layout, designed by Gary Bailey, is shown in Figure 32.

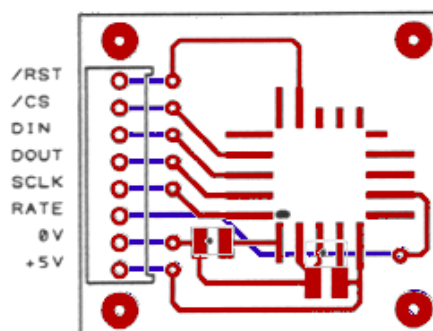


Figure 32: The gyro mounting board, designed by Gary Bailey using EasyPCB ECAD software. This is a double-sided PCB with hand-soldered vias; red denotes traces on the top of the board, blue denotes traces on the bottom. The gyro is mounted upside down in the centre of the square of pads; wires then connect it to the traces on the board.

# Photographs of assembled circuit boards

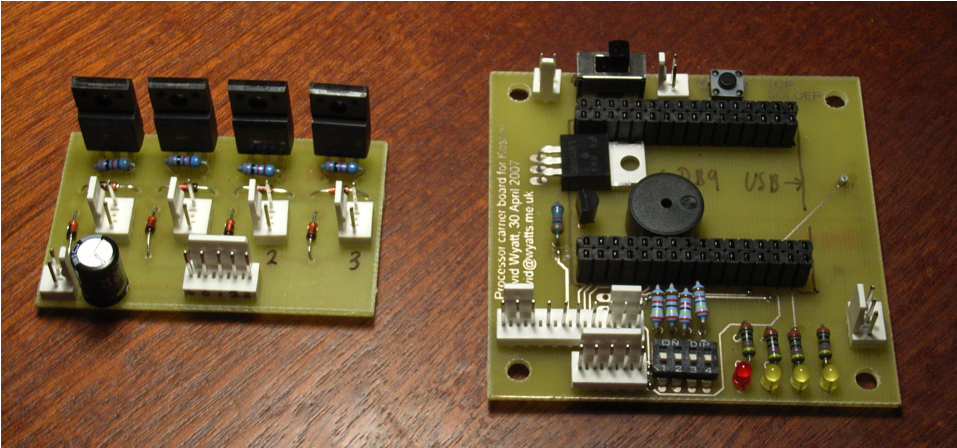


Figure 33: The valve driver board (left) and main avionics board (right), fully populated. The two ranks of header sockets on the avionics board accept the processor module.

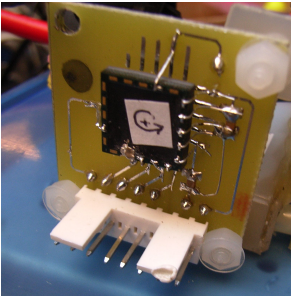


Figure 34: One of the two gyro boards installed on the rocket. The label is a mnemonic to record the direction of rotation that gives a positive output.

## Writing the report

### To do

????recovery system

????list software used in appendix?

## Control of transverse translation

For a rocket-powered vehicle that is required to move transversely (perpendicular to the direction of the rocket thrust), there are two main methods to achieve this:

1. Application of one or more forces whose resultant is a force in the desired direction at the centre of mass. Such forces could be applied by small attitude thrusters; the vehicle is treated as a 'free' mass since the rocket motor negates the gravitational attraction, analogous to a puck on an air-table.
2. Application of torques to tilt the main thrust vector such that it has a component in the desired direction. If the magnitude of the thrust is not increased, its reduced vertical component will lead to a loss of altitude of the vehicle. This is analogous to a helicopter or to a boat on a fast-flowing river.

Approach 2 has the problems both of loss of altitude during traverse manoeuvres and of increased difficulty in the control of the vehicle; however, it has the advantage of approach 2 that it can be implemented using no additional actuators compared with approach 1. Thus to the extent that transverse translation was considered in the design of the vehicle, approach 2 was taken.